GLOBAL CCS INSTITUTE

GOBIERNO DE ESPAÑA · MINISTERIO DE INDUSTRIA, ENERGÍA Y TURISMO

Strategies for injection of CO_2 into carbonate rocks at Hontomin

Final technical report

JUNE 2015

Authors:

T.Kovacs, Daniel .F. Poulussen and C.de Dios

CIUDEN

Collaborators:

Linda Luquot, Maarten Saaltink, Jesús Carrera, Berta Gómez, Sheila Fernandez, Victor Bezos, Yoar Cabeza, Silvia de Simone, Lurdes Martinez

SUMMARY

The OXY-CFB-300 Compostilla Project, partially funded by European Energy Programme for Recovery (EEPR), is a two phase project: firstly relating to technology development for the whole CCS chain; secondly related to demonstration and construction of an integrated commercial project. The partners in this project were Endesa, Foster Wheeler Oy and CIUDEN. Within the Technology Development Phase, CIUDEN managed the development of various facilities, including an oxyfuel combustion pilot plant in Cubillos del Sil (Leon province, Northwestern Spain), close to the existing Compostilla power plant, and a Technology Development Plant (TDP) for carbon dioxide (CO_2) geological storage in Hontomin (Ponferrada, Burgos province, North Central Spain). Ciuden is the leading public developer of CO_2 capture, transport and geological storage technologies in Spain, and has designed, constructed and recently commissioned the above mentioned facilities. The TDP will study processes involved in the injection of CO_2 into onshore saline aquifers and assist in the development of necessary technologies and methodologies to enable the storage of CO_2 at industrial scale in Europe. However, the Hontomin site itself does not represent an opportunity for commercial scale storage.

In collaboration with other research organisations including UPC and CSIC-IDAEA, work at Hontomín will focus on key storage issues such as: reservoir characterization at relevant scales, evaluation of injection strategies, determination of the reliability of both deep and surface monitoring techniques, and establishment of protocols to assist operators in the development of monitoring plans.

The purpose of this report is to share project plans and activities to date, including reservoir characterization tests and associated implications for injection strategies in carbonate rocks.

The Hontomin storage reservoir comprises fractured carbonates and dolomites of lower Jurassic age, at a depth of approximately 1.5km. The reservoir is sealed above by very low permeability marls and below by anhydrites. As part of the TDP, two wells have been drilled: H-I (CO_2 injection well) and H-A (observation well).

The injection of CO_2 into fractured carbonate rocks for dedicated storage is unique in a European context, although considerable experience of injection into carbonates has been gained in North America in association with enhanced oil recovery (CO_2-EOR) operations; for example by the end of 2011, over 18Mt of anthropogenic CO_2 had been stored in the Weyburn oil field in Canada (Wildgust et al, 2013).

The report includes a literature review with an emphasis on two important considerations for CO_2 injection into carbonates:

1. CO_2 may dissolve into formation brines, causing acidification and possible dissolution of carbonate minerals within the reservoir; this phenomena would mimic naturally occurring processes in carbonate rocks, such as the development of karst terrains. Extensive dissolution of minerals could have significant effects on the structure and permeability of carbonate reservoirs.
2. Fluid migration through carbonate reservoirs often tends to be dominated by flow along fractures, rather than the through the rock matrix (i.e. between mineral grains). The porosity and permeability of fracture networks (termed ‘secondary’) is complex; in order to design injection schemes to utilize secondary permeability, an understanding of fracture distribution and stress regimes is important.

To address these issues, simulations of large scale injections have been undertaken with an emphasis on predicting carbonate dissolution. This work has been complemented by small scale laboratory testing, to better understand the conditions under which dissolution may occur. Results from the simulation work suggest that development of extensive cavities in carbonate reservoirs is unlikely, because buffering effects tend to reduce the rates of dissolution with time. The laboratory experiments

showed that dissolution rates and localized effects are controlled by both rate of brine flux and dissolution rate kinetics. Intermittent injection of CO_2 may also lead to different effects compared to continuous injection.

The report also examines injection strategies, based on research and characterization tests undertaken at Hontomin:

- 'Push-pull' injection tests can be used to improve reservoir characterization and study capillary trapping
- Supercritical (dense phase) injection, proposed as a reference benchmark
- Liquid phase (cold/dense) injection, as a possible means of reducing compression costs at the wellhead
- Pulsed (intermittent) injection, which may accelerate dissolution of CO_2 in brine

For each of the above strategies, operational issues were investigated and plume development simulated. Results of the analysis showed that liquid phase injection could bring cost benefit and mechanical stability advantages; the latter finding is noteworthy because cold fluid injection is widely regarded as a potential fracturing risk to the reservoir, because relatively cold CO_2 injection may cause instability and small microseismic events.

TABLE OF CONTENTS:

1. INTRODUCTION

1.1. BACKGROUND

CO_2 geological storage, as an essential element of carbon dioxide (CO_2) capture and storage (CCS) projects has reached industrial scale in sites including Sleipner (Norway), In-Salah (Algeria), and Decatur (USA). These sites represent examples approaching the ideal conditions for establishing a commercial site, following the criteria established in SACS (Chadwick et al. 2007). .Other smaller sites have also achieved notable results from CO_2 injection operations, including Otway (Australia), Ketzin (Germany), Nagaoka (Japan), Lacq (France) and examples within the Regional Carbon Sequestration Partnership of the US Department of Energy. These sites have developed operations at a scale below 100kton CO_2.

All the above sites have provided valuable information and experience under different reservoir conditions; for example shallow depths (Ketzin), greater depths (Lacq), or in areas with relatively high levels of natural seismicity (Nagaoka), but all have geological settings that may be appropriate for industrial scale operations.

CIUDEN has been establishing a Technology Development Plant (TDP) for CO_2 storage for several years. The onshore storage test site (Figure 1.1) is located near the village of Hontomín in Northern Spain, 20km north of the city of Burgos. The geological setting of Hontomín consists of a dome-like structure located in formations of lower Jurassic age: marls as the upper seal, carbonates and dolomites as the storage formation, and anhydrites as the lower seal. (M5 Report Milestone5 FPA041). CO_2 will be injected into the carbonates located between approximately 1,440m and 1,570 m depth.

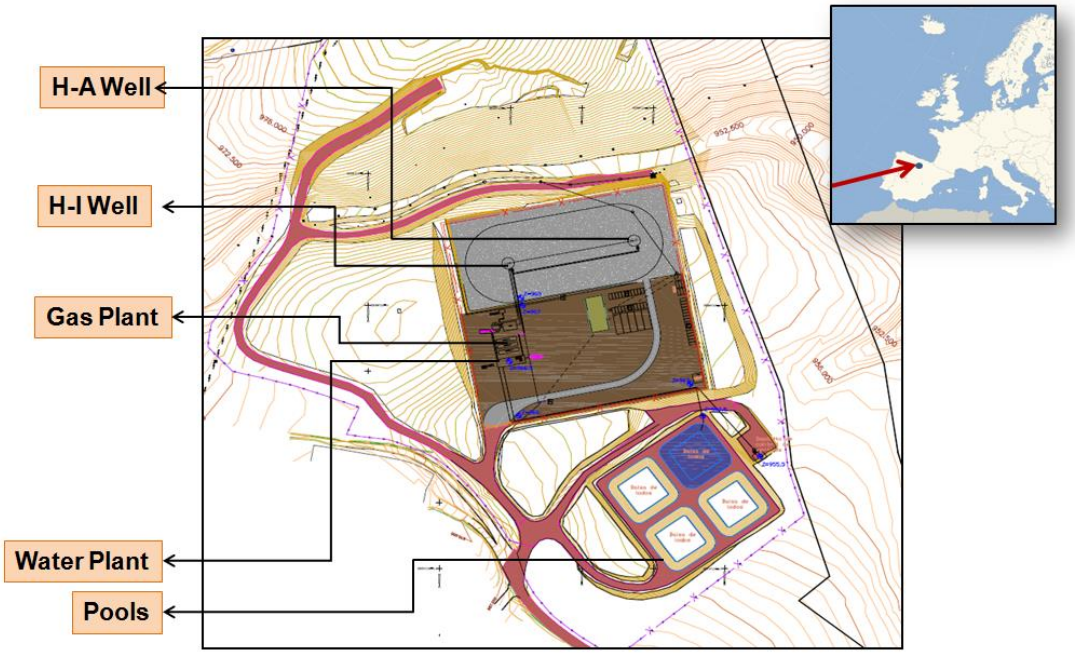

Figure 1.1: The Hontomín site schematic view and location (top), general view of **Hontomín** site and CO_2 injection well (bottom)

The site includes an injection well (H-I) and a monitoring well (H-A), both with total depth close to 1,580 m. Both wells are fully instrumented and further monitoring capabilities include a shallower hydrogeological monitoring network and a set of 30 surface micro-seismic stations.

CO_2 will be injected into a carbonate rock formation, which is unique in a European context; consequently, significant efforts have been devoted to characterization prior to injection. In order to obtain a first estimate of the permeability of the storage formation, a preliminary hydraulic characterization campaign was carried out immediately after drilling of the two wells (ref. Report Milestone 5 FPA041). The results of the campaign were also used to determine transmissivity (the product of reservoir permeability and thickness) and also assess possible effects of carbonate dissolution.

In well HA, transmissivity varied between 0.003m^2/d (which corresponds to a permeability of 0.015mD for the formation thickness of 165m) at low pressures (recovery period) and 0.04m^2/d (which corresponds to a permeability of 0.19 mD) at high pressures (injection period). Well HA displayed a significant skin effect. In well HI, transmissivity varied between 0.02m^2/d (which corresponds to a permeability of 0.12mD for the formation thickness of 133m) at low pressures and 0.3m^2/d (or 1.8mD) at high pressures (flow rate of 3L/s, and overpressure of 70bar at the well head). The well displayed some skin effect during the first injections, but this effect subsequently disappeared. These transmissivity values are two orders of magnitude lower than those reported by oil companies for two nearby oil exploration wells. Further characterization tests have been carried out in Hontomin, leading to a notable increase in permeability values in the reservoir. This underlines the need for extensive characterization of CO_2 storage sites in order to acquire a better understanding of the processes that will take place during operations.

HA well	**T (m^2/d)**	**k (mD)**	**Thickness (m)**	**P (bar)**	**Flow rate (l/s)**
Low P	0.003	0.015	165	50	3
High P	0.04	0.19	165	70	3
HI well	**T (m^2/d)**	**k (mD)**	**Thickness (m)**	**P (bar)**	**Flow rate (l/s)**
Low P	0.02	0.12	133	50	3
High P	0.3	1.8	133	70	3

Table 1.1. Pressures, flow rates and different transmissivity and permeability values from initial characterization tests at Hontomin. Further information in M5report FPA/041

1.2. OBJECTIVES

The purpose of this report is to share the plans and activities developed so far in characterization tests associated with different injection strategies in carbonate rocks, which will support the deployment of onshore CO_2 storage in Europe.

The objectives of this work are two-fold:

1) To summarize basic understanding about CO_2, carbonate rocks and their interaction. To this end, this report summarizes the literature on CO_2 thermodynamics, provides a succinct description of the huge literature on carbonate rocks and summarizes previous work on their interaction. Performance and interpretation of simulation models and laboratory tests to understand the dynamics of CO_2 injection and storage in carbonate rocks is also analyzed.

2) To describe strategies for CO_2 injection in carbonate formations. Specifically, (1) push-pull tests; (2) supercritical injection; (3) liquid phase injection; and (4) pulsed (intermittent) injection are discussed. For each of these, the shape and size of the CO_2 plume and operational conditions for low permeability formations, such as the one at Hontomín, are analyzed. Mechanical stability issues are also discussed.

Work at Hontomin will allow improvements against key issues for CCS development including the characterization of permeability at the scales relevant for CO_2 storage and the detailed analysis, by lab scale tests, modeling approaches and field scale tests for evaluation of different CO_2 injection strategies. The work has been undertaken in cooperation with key research organisations including UPC and CSIC-IDAEA.

2. BASICS CONCEPTS ON CARBONATE INJECTION

2.1 Introduction

This chapter covers the basic concepts for CO_2 storage in carbonate rocks. Thermodynamics of CO_2 are reviewed in section 2.2., whilst the nature of carbonate rocks is summarized in section 2.3. These two sections review existing knowledge, to frame the issue of CO_2 storage in carbonate rocks. The interaction between carbonate rocks and solutions rich in CO_2 during CO_2 storage is addressed in section 2.4.

An important feature of CO_2 injection into carbonate rocks is the relatively high solubility of carbonates (low permeability will not influence dissolution rate but rather cause localization of the dissolution process. If the permeability is low, dissolution will localize near the injection well). Injection of CO_2 in carbonates may in theory be problematic because of (1) the fast kinetics of carbonate dissolution, which explains (2) the tendency of carbonates to develop dissolution cavities, and is exacerbated by (3) the acidic nature of CO_2 solutions. Fluid accessibility to the reactive surface area is also a key parameter. If rock permeability is very low as at Hontomín, dissolution processes could be more localized. The following sequence of processes could be anticipated with injection:

1. CO_2 is injected as a liquid or supercritical fluid that displaces resident brine (multiphase flow).

2. CO_2 dissolves into the brine. In general, dissolution of CO_2 in water is controlled by Henry's Law, so that the concentration of aqueous (dissolved) CO_2 will be almost proportional to CO_2 pressure, which will be relatively high; therefore, the amount of dissolved CO_2 will also be relatively high at the brine-CO_2 interface. Reservoir temperature, pressure conditions, heterogeneity and brine salinity have to be highlighted as controlling factors.

3. Dissolution of CO_2 causes an increase in liquid density and leads to density driven fingers (e.g., Riaz et al, 2006; Hidalgo and Carrera, 2009; Pau et al, 2010). These fingers are important because they increase the interfacial area between the CO_2 and the brine, thereby accelerating the overall rate of dissolution of CO_2 into the brine. This is desirable because the brine saturated with dissolved CO_2 will tend to sink, counteracting the natural buoyancy of the CO_2 plume. As it turns out, the CO_2 rich brine loses most of its calcite dissolution capacity close to the CO_2 plume, which together with its tendency to sink makes this phenomena an effective trapping mechanism.

4. Dissolved CO_2 lowers the pH of the brine, which can dissolve carbonate minerals and change porosity, permeability and mechanical properties of the rock. Reactive transport modelling is necessary to understand, analyse and predict these interactions.

5. Carbonate dissolution neutralizes brine acidity, driving further dissolution of CO_2. This feedback process (dissolution of CO_2 in the brine causing acidity, and dissolution of the rock to neutralize acidity, followed by further CO_2 dissolution) would continue unchecked if it was not for the increasing build-up in bicarbonate and calcium concentration such that the brine remains at saturation with respect to calcite even at relatively low pH drops.

All of these steps imply that the actual amount of CO_2 (and carbonate rock) dissolved depends significantly on the respective fluxes of brine and CO_2, the interfacial area between brine and injected CO_2, and the reactive surface area of the carbonate minerals in contact with brine.

The processes and interactions described above are specifically relevant to carbonate formations, and provide the motivation for research at the Hontomin site. Note that the amount of supercritical CO_2 that

dissolves in the water may be partly controlled by carbonate mineral dissolution. Vice versa, the amount of mineral dissolution may be largely controlled by supercritical CO_2 dissolution into the brine. In theory, a relatively rapid rate of carbonate dissolution could result in large dissolution cavities to form in the formation, in turn compromising mechanical stability and creating fast flow paths for CO_2 migration away from the storage site. Therefore, CO_2 storage in carbonate rocks must accurately address reactive transport. A corresponding problem, however, is that carbonate dissolution observed in natural rocks tends to be concentrated, creating cavities, caverns, and preferential subsurface flow paths (wormholes). Therefore, understanding the problem requires both large-scale simulations, to understand how much rock can be dissolved, and small-scale experiments, to understand the conditions for dissolution localization; potentially leading to a better definition of the plans to be developed at field scale in Hontomin.

2.1. CO_2 PURITY

Operational conditions change significantly during the capture, compression, transportation, injection and storage stages of CCS projects; typical pressure and temperature ranges are listed in Table 2.1 below. CCS projects must be designed with an understanding of thermodynamic properties, such as density and viscosity, under these conditions. This section broadly describes the thermodynamic properties of pure CO_2 and CO_2 streams with impurities originating from capture processes.

Table 2.1: Estimated operation conditions (P and T) of the CCS processes (Table 2.2 from Hailong Li, 2008).

CCS process	Range	
	Pressure (bar)	Temperature (K)
CO_2 compression/purification	*0 – 110*	*219.15 – 423.15*
Initial compression	0 – 30	293.15 – 423.15
Dehydration	20 – 30	289.15 – 303.15
Purification	20 – 50	219.15 – 248.15
Further compression/pumping	50 – 110	283.15 – 303.15
CO_2 transportation	*5 – 200*	*218.15 – 303.15*
Pipeline	75 – 200	273.15 – 303.15
Small tanks	15 – 25	238.15 – 248.15
Large tanks	5 – 9	218.15 – 228.15
CO_2 storage	1 – 500	277.15 – 423.15

Explanatory note: Whilst pressure, temperature in capture, compression and transport are governed by engineering requirements, injection/storage will be partly controlled by natural factors such as depth, geothermal gradient, etc.

2.1.1. Pure CO_2

The CO_2 phase diagram (Figure 2.1) shows distinct solid, vapor, liquid and supercritical (or dense) phases with peculiar behavior at two points: the triple point and critical point. The triple point (about -56.6°C, 5.18bar) is defined as the temperature and pressure at which solid, liquid and gas phase are able to coexist in equilibrium. From the triple point, the melting and saturation lines separate solid/liquid phases and the liquid/vapor phases, respectively. The saturation line links the triple point to the critical point. Above its critical temperature (31.1°C) and pressure (72.9bar), pure CO_2 takes on the properties of a supercritical fluid, where viscosities and diffusivities are close to those of gases, and densities close to that of a liquid. In case of CCS, the conditions will be around the saturation line and below critical point, having the CO_2 in gas, liquid and supercritical phase, depending on the project. If

we focus on the storage part, the supercritical state is likely to be the most suitable, in order to maximize the efficient use of pore space

There are some features of CO_2 thermodynamics that should be noted:

- The Joule-Thompson effect could take place in an isenthalpic expansion, where no enthalpy is exchanged. The temperature can change when the potential energy of the bonds between molecules changes when a real gas changes to an ideal gas, or vice versa. This effect is quantified by means of the Joule Thompson coefficient (ºC/bar) and is very sensitive to pressure and temperature variations and in the case of CO_2 the coefficient is higher than that of other common gases.

Figure 2.2 shows various thermodynamic properties of pure CO_2 as a function of pressure and specific enthalpy.

In Hontomín, CO_2 could become liquid during injection into the first 700 meters of the well. Under these conditions, temperature will be between 5 ºC and 31 ºC and pressure between 50 bar and 73 bar, and density will vary, but will always be less than that of the brine.

As CO_2 approaches supercritical conditions, the meniscus between liquid and gaseous CO_2 disappears. A supercritical fluid can diffuse faster in a solid matrix than a liquid, yet possess a solvent strength to extract the solute from the solid matrix (Akgerman et al, 1994). In the case of Hontomín, supercritical conditions for CO_2 exist from 700 to 1,500 meters depth.

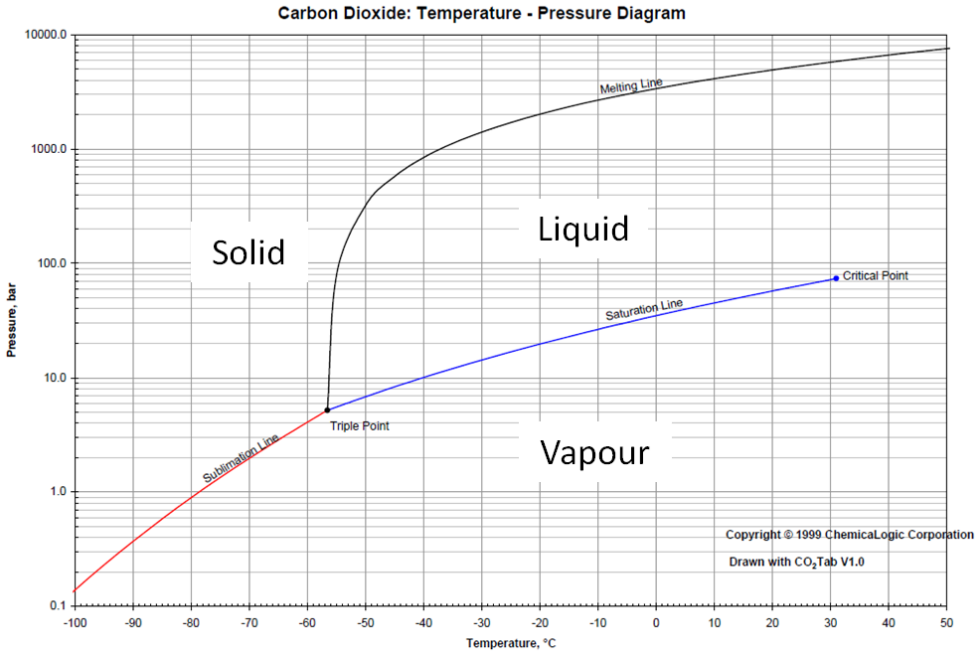

Figure 2.1: Phase diagram showing the various phases of pure CO_2 at given pressures and temperatures (ChemicaLogic, 1999).

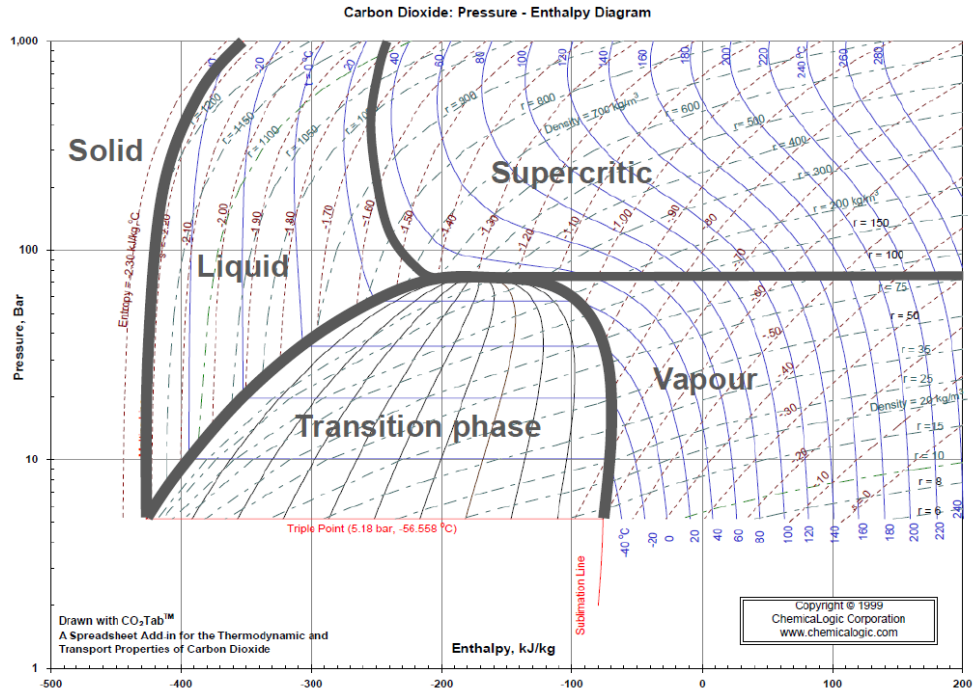

Figure 2.2: Mollier diagram (Pressure-Enthalpy-Density-Temperature-Entropy diagram) for pure CO_2 based on experimental data (ChemicaLogic, 1999). This diagram relates pressure (bar, log scale, x-axis), specific enthalpy (kJ/kg, normal scale, y.axis), temperature (Kelvin, blue lines), density (kg/m3, dashed green lines), specific entropy (kJ/kg, brown lines) and the state of matter (Zones separates by grey lines which perform sublimation, saturation and melting lines). Temperature, density and entropy are represented by iso-lines.

Figure 2.3 shows how density and viscosity change as a function of pressure and temperature. Near the critical point and under supercritical conditions, a small change in temperature can lead to a very large change in both density and viscosity. The same occurs for pressure changes.

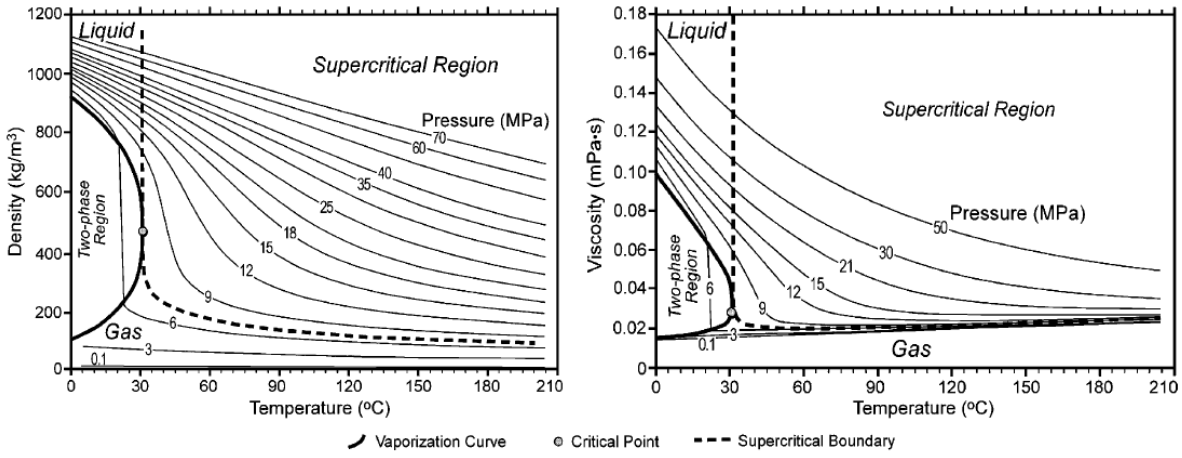

Figure 2.3: Density and viscosity values for pure CO_2 (Nordbotten et al, 2004).

To characterize fluid behaviour at different conditions, reliable equations of state (EOS) are needed to relate thermodynamic or other properties (density, viscosity, specific heat) with state variables such as pressure and temperature.

One can distinguish two kinds of EOS: specialized EOS, such as the Span & Wagner EOS for CO_2 and generalized EOS, such as the van der Waals EOS. Specialized equations have a better accuracy than generalized EOS, but are limited to specific substances. General EOS can be further divided into two types: equations with simple structures, such as Redlich-Kwong EOS; and equations with complex structures, such as Benedict-Webb-Rubin EOS (Hailong Li, 2008). Although the general equations with complex structure may give better results, as they contain more parameters, their calculation is more complicated, especially for some derived properties such as enthalpy and entropy.

Table 2.2 lists some open source and commercial software available for the calculation of various EOS that can be applied to both and impure pure CO_2 streams. For pure CO_2: they use various EOS, such as that of Redlich and Kwong (1949), Peng and Robinson (1976) and Span and Wagner (1996).

Table 2.2: Equations of State available in Software packages for CO_2 simulation (E-on report, 2011).

Software Package	Equation of State	Notes
Eclipse	N/A	Black Oil Methodology
GEM / STARS	PR (1) SRK (2)	Both 1976 and 1978 versions of PR available for "a" constant. Original and G&D "a" constants available for SRK.
HYSYS	PR SRK	
Multiflash	Span Wagner CSMA PR SRK	The CO2 high accuracy model uses SW for equilibrium properties for pure CO2 and corresponding states approach to determine the properties of mixtures.
Olga	Span Wagner	CO_2 can currently only be modelled as a pure component within Olga i.e. cannot model CO_2 mixtures.
Promax	Span Wagner PR SRK	Span Wagner may only be utilised for pure CO2 streams; mixtures should be modelled using PR or SRK
Prosper	PR SRK	

Explanation: Soave (1972) PR, Peng and Robinson (1976) and Span Wagner, Span and Wagner (1996), CSMA (a series of highly accurate equations for reference fluids).

The applicability of these various EOS to different CCS processes is discussed below.

In general, the Span Wagner EOS should be used to model the equilibrium thermodynamic properties of CO_2 necessary for studies of the flow in pipelines (at the injection wells or in transportation), because it is one of the most accurate thermodynamics laws for pure CO_2. However, the Span Wagner equation of state was designed for pure CO_2 and thus may only be used for CO_2 streams of very high purity. It is therefore not applicable to many capture plants, which will contain a mixture of process gases for which a number of reliable proven EOS and models exist that deal with the Vapor Liquid Equilibrium (VLE) and other parameters affecting thermodynamics.

2.1.2. Impure CO_2

With reference to the phase diagram for pure CO_2, melting and saturation lines and critical temperature and pressure can vary according to the chemical composition of the CO_2 stream obtained from capture processes. Therefore it is important to assess the effects of impurities on thermodynamic properties.

The capture process within CCS projects determines the fluid composition which will be transported and finally stored, but some level of impurity will always be present. The CIUDEN Compostilla oxycombustion capture process has been chosen as the reference scenario in this report. This process consists of fuel combustion with essentially pure O_2 rather than air, yielding an almost nitrogen-free mixture in the boiler, then CO_2 can easily be processed to produce pure CO_2, once flue gas cleaning and CPU processes are applied. This promising technology allows the purest composition of CO_2 in the fluid exiting the boiler, despite the need for previous oxygen production. The concentrations of non-condensable gases such as N_2, Ar, and O_2 in various CO_2 streams and other types of impurities will vary due to redox conditions in the CO_2 streams. Table 2.3 shows the expected flue gas composition of the CIUDEN capture plant in Cubillos del Sil, León.

Table 2.3: Expected CO_2 stream composition from Oxycombustion, before flue gas cleaning and CPU processes (Cortés et al, 2013).

% vol	N_2	CO_2	H_2O	O_2	VOL REL	IMPURITIES
FUEL + O_2 (30%) + CO_2	6	83,5	7	3,5	65	SOx NOx PARTICLES

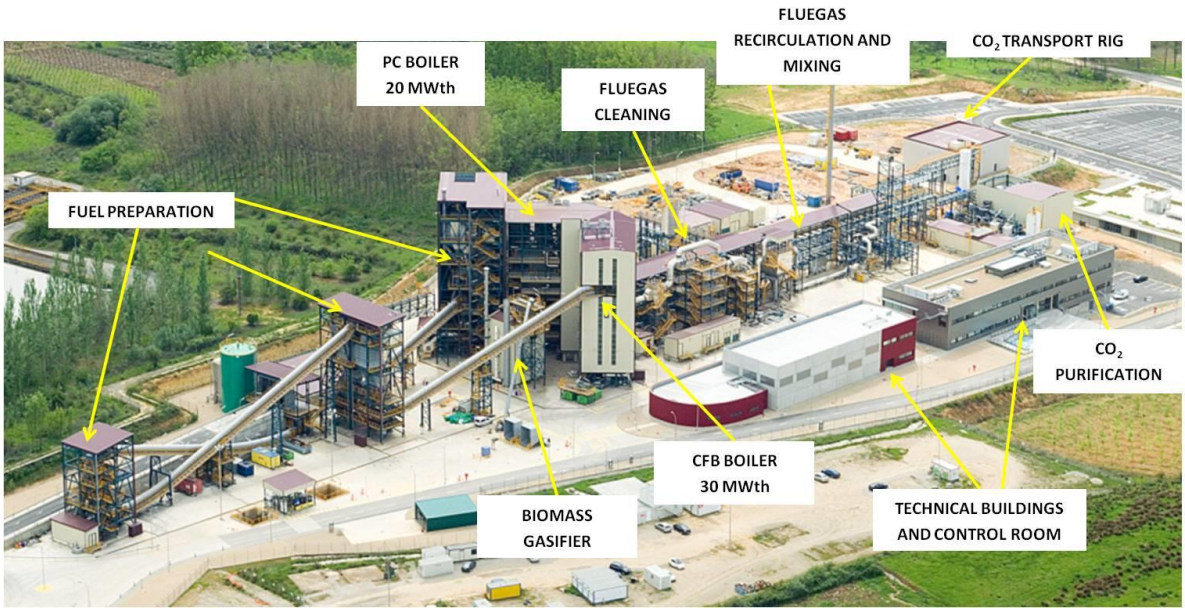

Fig 2.4. CIUDEN CO_2 Capture Plant

There are no major technical barriers to providing high purity CO_2 from the flue gas of fossil fuel power plants. However, high purity requirements may induce additional costs and energy requirements resulting in a loss of power plant efficiency. Hence, it is important to find an optimal balance amongst requirements from purification, transport, storage, legal and environmental aspects.

Therefore, impurities including N_2, O_2, Ar, H_2O, CH_4, SO_2, and H_2S are usually accounted for in the study of the thermodynamic properties of CO_2 streams in CCS projects.

The effects of impurities on EOS can be seen in Fig.2.5. The phase diagram and the critical points change according to the proportion of N_2 in the CO_2 stream. Moreover, CO_2-N_2 streams will exhibit a contour that envelopes a vapour liquid equilibrium (VLE) region as opposed to a saturation line in the case of pure CO_2 (blue line in the figure). For a pure substance, vapour pressure at a given temperature is constant and therefore P-T plots as a single line; whereas for a mixture of given composition at a given temperature, vapour pressure is not a fixed quantity and varies between dew point pressure (DPP, pressure point where the fluid state shifts from liquid to vapour) and bubble point pressure (BPP, pressure point where the fluid state shifts from vapour to liquid). Similarly, at a given pressure the phase change occurs over a range of temperatures from bubble point temperature (BPT) to dew point temperature (DPT). Thus vaporization of mixtures requires two curves on the P-T diagram.

Hence, this expansion of the liquid–vapour phase envelope is related to the start of boiling (in liquid) or condensation (in vapour) at relatively higher pressures. Moreover, fluid properties (such as density) will evolve gradually during the transition phase of the mixture depending on the mole fraction of each component.

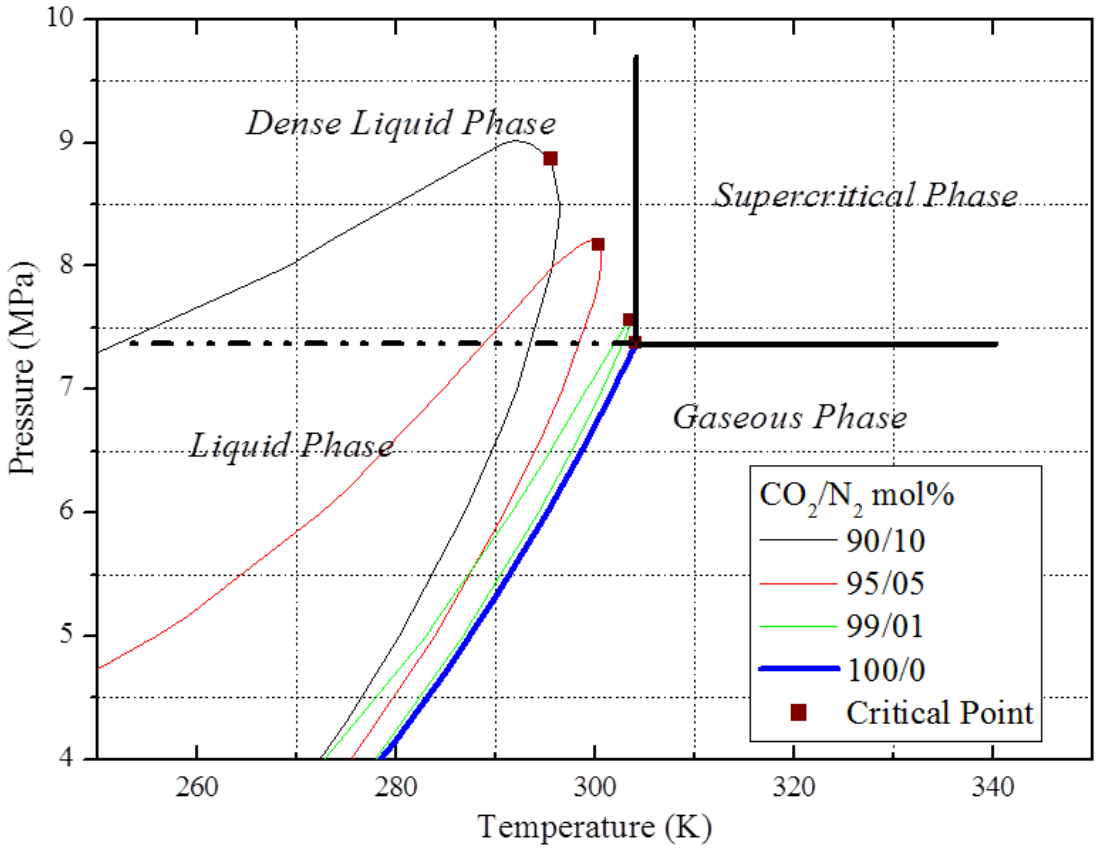

Figure 2.5: Impurity impact example: Movement of critical points in the phase diagram, pure-CO_2 versus binary system of CO_2/N_2 (Yan and Thorin, 2008).

Impurities can affect CO_2 stream equilibrium behaviour/VLE, pressure-volume-temperature (PVT) and transport properties such as viscosity, density and hydrate stability.

There are two types of thermodynamic methods used for calculations of phase equilbrium: liquid activity coefficient based models and EOS based models. According to Hailong Li (2008), activity

coefficient models are the best way to represent highly non-ideal liquid mixtures at low pressures, and can be used to describe mixtures of any complexity. The EOS methods can be applied over wide ranges of temperature and pressure, including sub-critical and super-critical regions.

In order to consider the wide range of operational conditions of CCS processes (Table 2.1), EOS will be more applicable than activity coefficient methods.

As explained in the previous section, reliable models to predict VLE are essential for designing CO_2 transport and injection. Reliable data on VLE and physical properties for CO_2 streams are essential to design the necessary purification processes, compression and transportation.

Several authors have studied available EOS for the design of CO_2 pipelines (Hailong Li, 2008; Coquelet et al, 2008; Goos et al, 2011, Al-Siyabi, 2013; Ahmad et al, 2014), and have included experimental data to check the accuracy of models based on EOS.

The effects of impurities on density and viscosity has been assessed based on variousreports and studies (e.g. Eriksson, 2009 and GCCSI 2009). In order to compare and check EOS models, properties have been calculated by the software programs HYSYS and ProMax (see Table 2.2 for more details and Project, E. U, (2011)). Both programs used models based on the Peng-Robinson EOS for impure stream samples; whilst for the pure CO_2, HYSYS has adopted Peng-Robinson and ProMax used Span & Wagner. Noting that a general cubic equation should be used for impure streams rather than a specialized equation such as Span & Wagner, Figure 2.6 and 3.7 show variations in density calculated by HYSYS and ProMax, respectively.

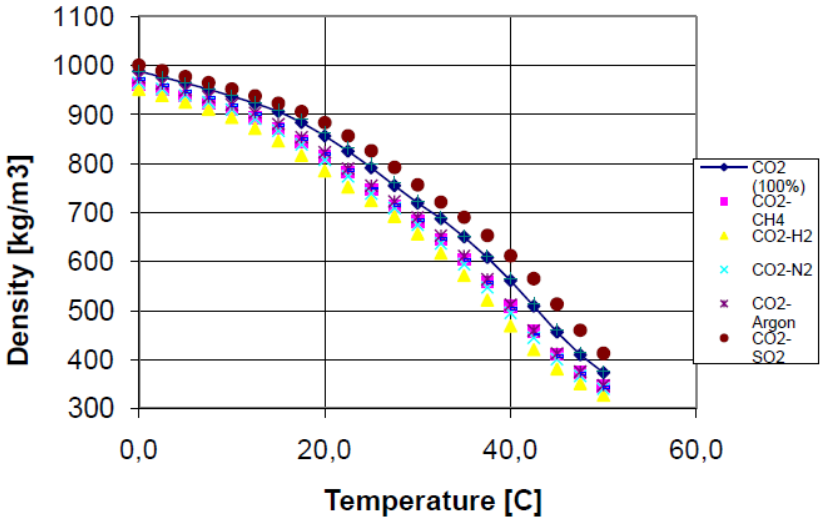

Figure 2.6: Effects of Impurities for Density versus Temperature at a Constant Pressure of 100 bar using HYSYS.

As expected, both model results produce similar results for any given binary CO_2 mixture. The respective stream compositions used to make the binary mixture diagrams comprise 98 mole% CO_2 and 2 mole% of the other component; pure CO_2 is also plotted for comparison.

Figures 2.6 and 2.7 indicate that only SO_2 will increase the density of streams compared to pure CO_2; of the other impurities which all decrease density, H_2 shows the most significant effect. Since the composition obtained from oxy-combustion capture contains a moderate percent of N_2, a modest decrease in density compared to pure CO_2 could be anticipated, under the conditions assumed.

Figure 2.8 and Figure 2.9 show differences in viscosity caused by various impurities, with the same set of binary mixtures already described above for Figures 2.6 and 2.7. Both figures show that SO_2 will increase viscosity slightly in comparison to pure CO_2, whilst all other binary mixtures exhibit a decrease. This indicates that impurities typically will reduce the viscosity of supercritical CO_2 streams (dense phase, T > 31.1 ºC). Figure 2.9 shows irregular behaviour between 25 and 35 °C because ProMax uses the Supercritical model for vapour.

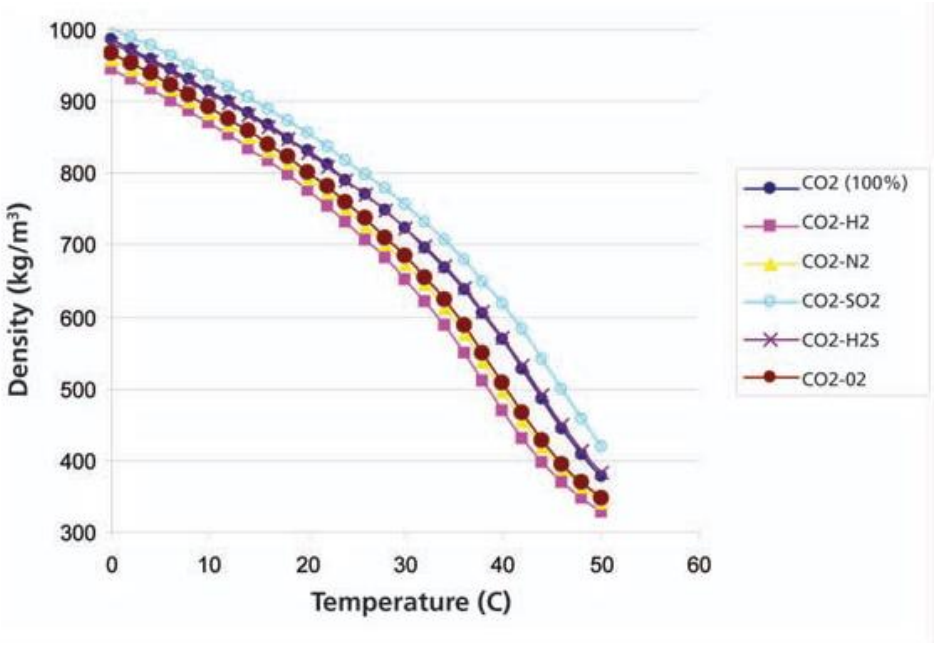

Figure 2.7: Effects of Impurities for Density versus Temperature at a Constant Pressure of 100 bar using ProMax.

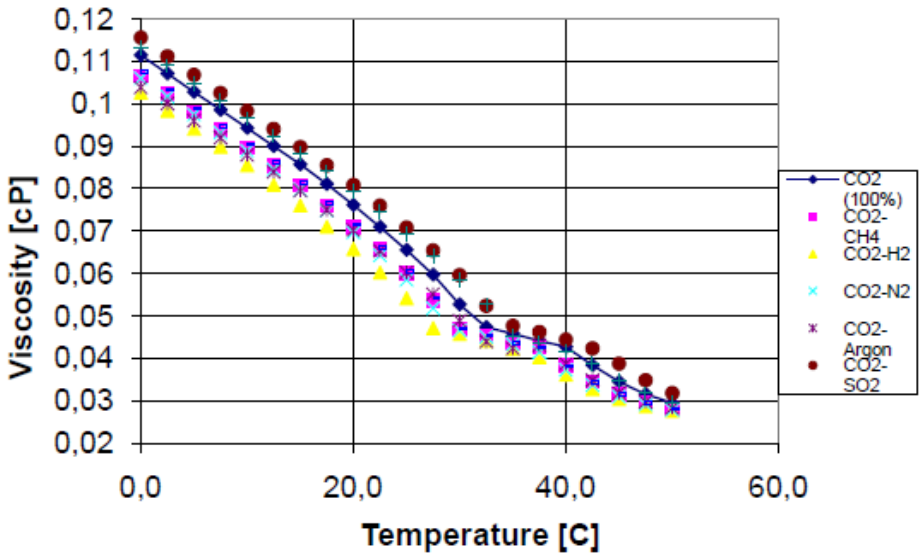

Figure 2.8: Effects of Impuritiesfor Viscosity versus Temperature at a Constant Pressure of 100 bar using HYSYS.

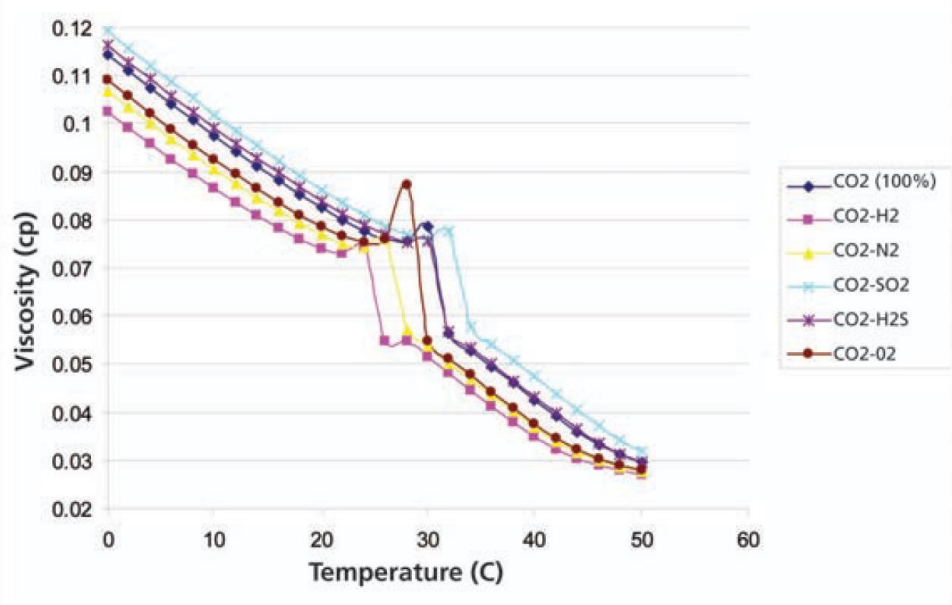

Figure 2.9: Effects of Impurities for Viscosity versus Temperature at a Constant Pressure of 100 bar using ProMax.

The formation of hydrates presents another potential issue for transport and injection of CO_2 streams, although dehydration of captured streams renders corrosion and hydrate formation issues unlikely during the transport stage of CCS projects. The presence of impurities could affect hydrate formation during injection, although conditions at the Hontomin site are not anticipated to favour hydrate formation.

Further approaches are going to be tested at a sizable scale in CIUDEN´s experimental transport test rig (Fig. 2.10) in the frame of the EU FP7 project "IMPACTS" (http://www.sintef.no/Projectweb/IMPACTS/).

Fig. 2.10 Ciuden experimental transport test rig

2.2. CARBONATE ROCKS

2.2.1. Introduction

Carbonate sediments are commonly formed in shallow, warm oceans either by direct precipitation out of seawater or by biological extraction of calcium carbonate from seawater to form skeletal material. The result typically consists of particles with a wide range of sizes and shapes mixed together to form a multitude of depositional textures. The sediment may be bound together by encrusting organisms or, more commonly, deposited as loose sediment subject to transport by ocean currents (Petrowiki website).

It is estimated that more than 60% of the world's oil and 40% of the world's gas reserves are held in carbonate reservoirs (Sheng, 2013). The Middle East, for example, is dominated by carbonate fields, with around 70% of oil and 90% of gas reserves held within these reservoirs. Carbonates can exhibit highly varying properties (e.g., porosity, permeability, flow mechanisms) within small sections of the reservoir, making them difficult to characterize. A focused approach is needed to better understand the heterogeneous nature of the rock containing the fluids and the flow properties within the porous and often fractured formations. This involves detailed understanding of the fluid saturation, pore-size distribution, permeability, rock texture, reservoir rock type, and natural fracture systems at different scales. Fracture corridors often exist that range from tens to hundreds of meters in width and height

and have a real extent in the order of kilometres, representing primary pathways for fluid migration. Such fracture corridors can have a permeability of a thousand times greater or more than the surrounding rock matrix and have a considerable impact on oil, gas, and water production, including issues related to the drilling process (Schlumberger website).

2.2.2. Petrophysical properties

Porosity, permeability, and bulk density depend on fundamental properties such as texture, mineralogical composition, and fabric. Porosity and permeability are among the most important variables that determine reservoir quality, and thus are of key interest for CO_2 storage. While rocks are classified according to their fundamental properties and inferences are made from rock classifications about depositional environments, porosity is classified according to physical attributes that may not be related to mode of origin.

Porosity is measured directly from core samples and indirectly with various borehole logging tools. Permeability is measured as the coefficient of proportionality in Darcy's equation for fluid flow through porous media. It is measured directly from core samples (fig. 2.11) and it is the yardstick by which many quality rankings are assigned to reservoirs.

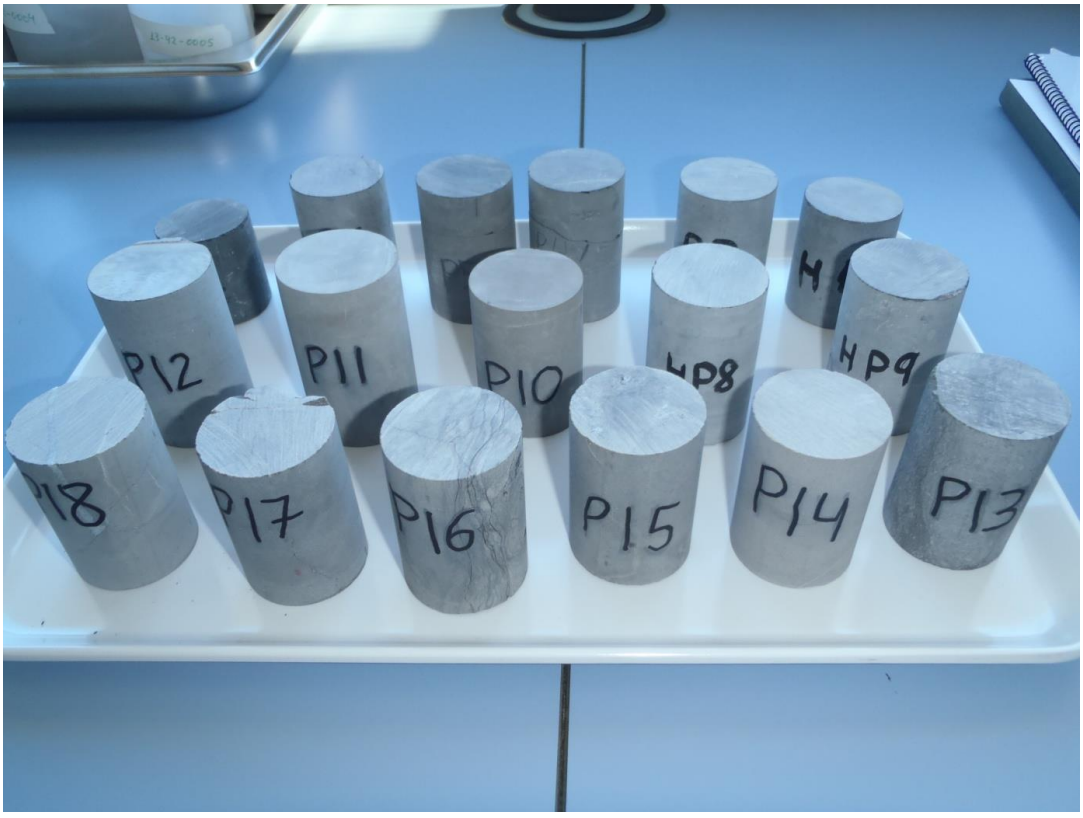

Figure 2.11. Core samples from Hontomin site

Porosity

Porosity is the ratio of voids to sample volume. It is usually designated by the symbol □ and expressed as a percentage:

□ = $(V_p/V_t)\times 100$

with V_p the pore volume and V_t the total rock volume.

Reservoir specialists are primarily concerned with the fraction of total porosity that transmits fluids, that is, the interconnected or effective porosity; ϕ_e. Effective (connected) porosity is the ratio of the interconnected pore volume to the total rock volume. Direct measurements of Vp in the laboratory are measurements of effective porosity. Not all pores are interconnected, however. Unconnected porosity is called residual porosity, ϕ_r, so that total porosity is the sum of $\phi_e + \phi_r$. (see Wayne M. Ahr, 2011, for more details).

Porosity varies with texture, fabric, and fracture geometry in the reservoir rock. Grain shape, sorting, and packing are the main variables that affect porosity in clastic rocks, growth fabric and skeletal microstructure affect inter - and intra-particle porosity in biogenic rocks, and porosity in fractured rocks is determined by fracture width, fracture spacing, and presence/absence of mineralization. Diagenesis may plug pores with cement, close pores with compaction, open pores with dissolution, or create new pores by recrystallization or replacement. Berg (1970) illustrated the geometrical relationship between pore size and grain size with identical spheres in a packing arrangement with about 30% porosity.

Porosity in modern carbonate sediments ranges from about 40% to 70% but is about 5% – 15% in ancient rocks (Choquette and Pray, 1970). Porosity reduction is complex and can involve cementation, compaction, or combinations of the two.

Porosity is a measure of capacity to store fluids; permeability is a measure of capacity to transmit fluids. Pores are connected by pore throats, which strongly influence permeability and which are related to pore size, shape, and arrangement. If one rock is composed of spherical, well - sorted grains of a given size, inter-granular pores will be only a fraction of the grain size and the attendant pore throats will be even smaller but generally uniform in size. Rocks with poorly sorted grains will have poorly sorted pore and pore throat sizes. Sorting and distribution of pore throat sizes in rocks determines pore – pore throat size ratio and accessibility of fluids to the pore throat system in rocks.

In most carbonates, pore and pore throat geometries are not as predictably regular as this ideal case; therefore it is helpful to be able to identify the pore types that have the most influence on permeability. In order to understand pore characteristics and how pore types are related to other readily identifiable rock properties, a system for classifying carbonate porosity is necessary.

Porosity Classifications

A simple classification for porosity might designate three categories of pores as interparticle, vug, and fracture. A tiered classification scheme might group according to average pore size, pore shape, petrophysical characteristics, and mode of origin.

Traditional classifications of carbonate porosity were not designed for that purpose, but the well-known schemes by Archie (1952), Choquette and Pray (1970), and Lucia (1983) are useful to illustrate the evolution in thinking about carbonate reservoir pore systems. Finally, a new classification based on end-member genetic categories—depositional, diagenetic, and fracture porosity—is presented as a more useful alternative.

The Archie porosity classification Archie (1952) is based on textural descriptions of reservoir rock along with the “character” of any visible porosity. Three textural categories are termed Type I, II, and III, and four classes for visible porosity are identified as classes A through D. Class A has no visible porosity at 10 magnifications, class B has visible pores between 1 and 10μm, and class C has visible pores larger than 10μm but smaller than rotary cuttings (roughly, about 2.0mm). Class D includes large visible pores such as solution vugs larger than cuttings samples.

Archie described Type I carbonates as “crystalline, hard, dense, with sharp edges and smooth faces on breaking. For practical purposes, these rocks correspond to today’s mudstones and dolo-mudstones. Type II rocks are described as “earthy” or “chalky” with grains not larger than about 50μm in diameter (just below the finest silt size), and they are composed of “ fine granules or sea organisms. These rocks correspond to today’s true chalk, or mudstones and wackestones that have probably undergone diagenetic alteration to attain the chalky appearance. Type III carbonates are “granular or saccharoidal.” The major contribution of the Archie classification is that it relates petrophysical properties, including capillary pressures, electrical properties, and saturation characteristics, to different rock types.

Choquette and Pray (1970) (Figure 2.) recognized the need to incorporate time and mode of origin in their classification of carbonate porosity. They recognized 15 basic pore types and organized them into three classes depending on whether they are fabric selective, not fabric selective, and fabric selective or not. The origin of fabric-selective pores could be depositional, diagenetic, or both, although that point is not emphasized in the classification. Intergranular pores in an oolite grainstone, intercrystalline pores in a crystalline dolomite, or grain - moldic pores in a skeletal packstone are examples of fabric-selective pores that have different origins. Non-fabric-selective porosity includes fractures or dissolution cavities of various sizes that cut across rock fabric. Fabric selective or not is a category that includes mainly penetrative features such as animal or plant borings and burrows and desiccation cracks.

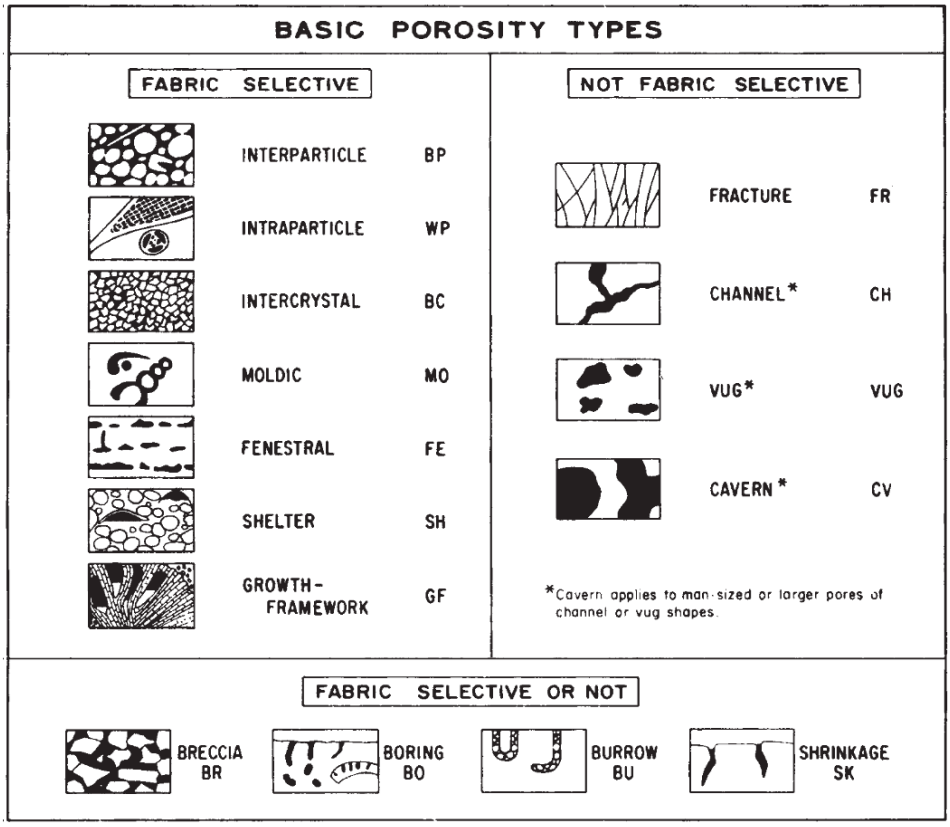

Figure 2.12: The essential elements of the Choquette−Pray (1970) porosity classification for carbonate rocks. The essence of the classification is whether or not porosity conforms to rock “fabric”. Note that rock fabric in this sense includes both depositional and diagenetic fabrics. (Adapted from an illustration by Choquette and Pray (1970) in Scholle (1978)).

Lucia's (1983) classification of carbonate porosity (Figure 2.) evolved from work done at Shell Oil and Shell Development Companies during the 1960s. Although the influence of Archie's work is evident in Lucia's classification, Lucia's division of carbonate pore types into vuggy and interparticle categories distinguishes it. Like Archie, the objective of Lucia's classification is to provide a practical field and laboratory method for visual description of porosity in carbonate rock samples. For rocks with interparticle and separate vug porosity, Archie's m factor can be estimated if the particle size, amount of separate vug porosity, and total porosity are known. Lucia's emphasis on the relationship between porosity, permeability, inferred capillary displacement pressure, and particle size, some of which relationships were also recognized by Craze (1950) and Bagrintseva (1977), is an early method for "rock typing" or ranking reservoir zones on the basis of petrophysical characteristics.

A particularly important attribute of Lucia's classification is its emphasis on the petrophysical significance of separate and touching vugs, which are pores larger than surrounding framework grains. They may have originally been moldic, interparticle, intraparticle, or intercrystalline pores, but they were enlarged by dissolution to become vugs.

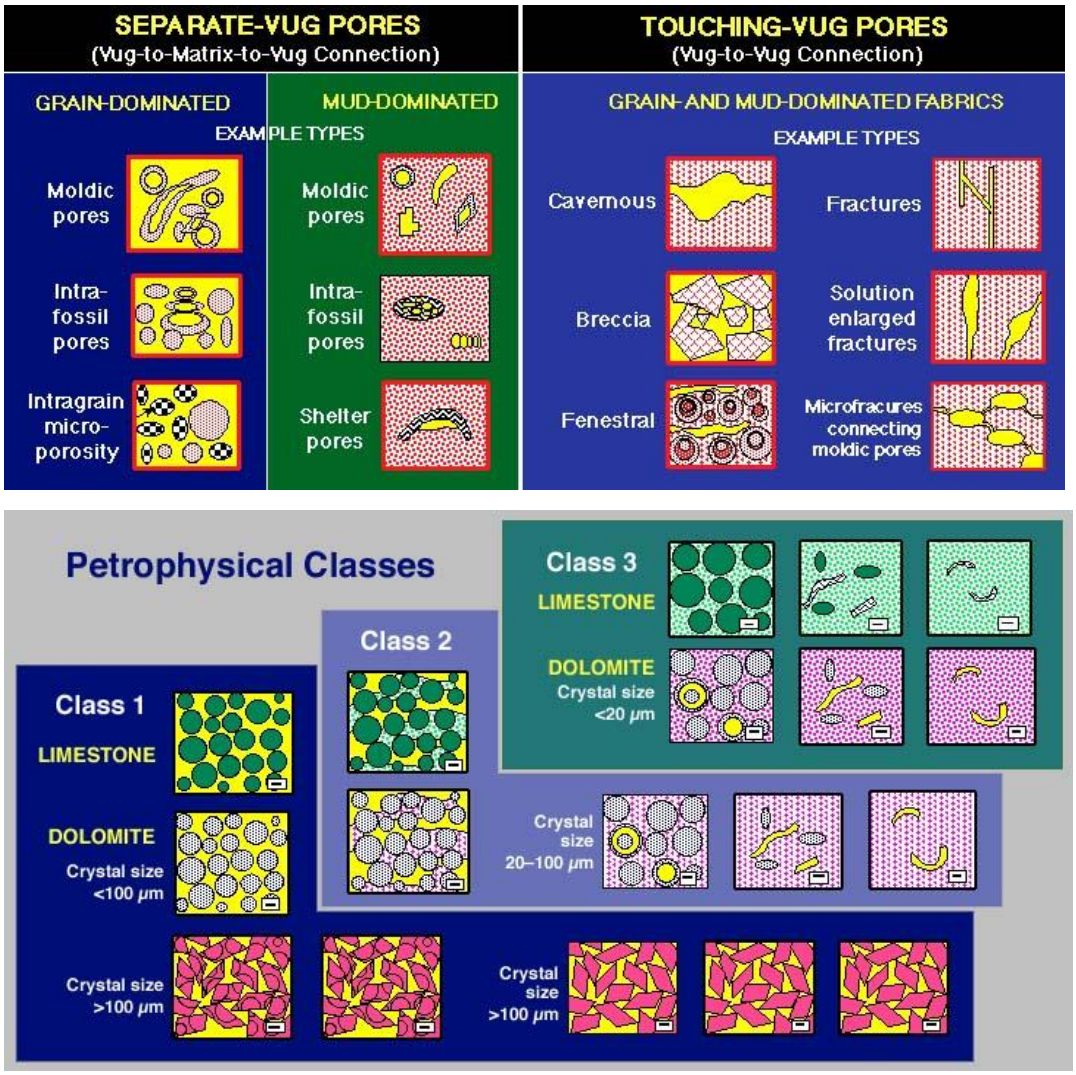

Figure 2.13: Classification of carbonate porosity by Lucia (1983). This scheme is especially important because it emphasizes that interparticle (grains or crystals) porosity and separate or touching vuggy porosity have profound effects on such reservoir petrophysical characteristics as Archie's *m* (cementation exponent), porosity−permeability relationships, and capillary pressure behavior. The latter influence is reflected by the "P_d" values in psi, which indicate the mercury displacement pressure required to enter the pore systems corresponding to small, intermediate, and large particle sizes.

Non-vuggy or interparticle pores are classified by Lucia as visible or not visible in cuttings. Visible pores are grouped according to particle size as fine (<20 μm), medium (20-100 μm), and large (>100 μm).

Recently, Lonoy (2006) incorporated basic elements of Lucia's (1983, 1995) and Choquette and Pray's (1970) classifications into a porosity evaluation scheme based mainly on statistical correspondence between porosity and permeability in various Lucia and Choquette–Pray pore types. Lonoy (2006) added subdivisions of pore categories in both classifications to create additional varieties of interparticle and intergranular pore types. He added refinements to better distinguish macro–and micromoldic pores, and created additional categories for microporous, mud-supported fabrics. Lonoy's (2006) study provides valuable information about correspondence between porosity and permeability in different carbonate pore types and it should provide useful information for refining pore volume estimates used in volumetric calculations.

Permeability-Porosity relationship

The porosity/permeability relations in rocks are widely used in practice, mainly because permeability is a "no-logging parameter": despite all attempts (and the corresponding publications), there is no reliable log analysis method to continuously measure the permeability of the reservoir rocks in the borehole. As a result, porosity-permeability relations are needed to obtain preliminary estimates of permeability. It must be kept in mind, however, that actual permeability depends on other factors (most notably pore size and connectivity), that are not captured by porosity. As a result, these expressions are highly uncertain and need to account for these additional factors (fig. 2.14).

Discrete hydraulic methods are obviously available (e.g. mini-test), but they are costly. Reservoir geologists therefore would like to find a relation between porosity (easily measured using log analysis techniques) and permeability, so that it can be easily deduced. Most of the time, this is a risky operation. The complexity of the □-k relation is related to the complexity of the porous space itself.

Carbonates often show highly heterogeneous and tortuous pore networks. This means that a conversion from porosity to permeability and multi-phase flow properties is far from straightforward (Blunt etal., 2012, Gomes etal., 2008, Hamon, 2003 and Neilson and Oxtoby, 2008). Carbonate pore systems do not divide in a unique manner into pore bodies and pore throats, but rather are variously-scaled, complex pore systems that challenge such a simple classification. While several pore classifications have been proposed (e.g. Choquette and Pray, 1970, Mousavi etal., 2013, Lønøy, 2006 and Lucia, 1995), these are based on petrographically observable textures alone and are not specifically related to single- and multi-phase flow properties of the rocks themselves.

The petrophysical properties of carbonates and the distribution of these properties within the subsurface, result from the original sediment grain type and fabric, the depositional architecture, and the diagenetic and structural events imposed during burial and/or uplift. Due to their highly reactive nature, carbonate rocks often display a strong post-depositional overprint (Fig.2.15). Diagenetic processes such as cementation, neomorphism, dissolution, compaction and dolomitization can reduce or enhance porosity, so redistributing pore space and changing its relative volume, so altering both porosity and permeability as well as the multi-phase characteristics of the final carbonate rock (Flügel, 2004 and Lucia, 2007).

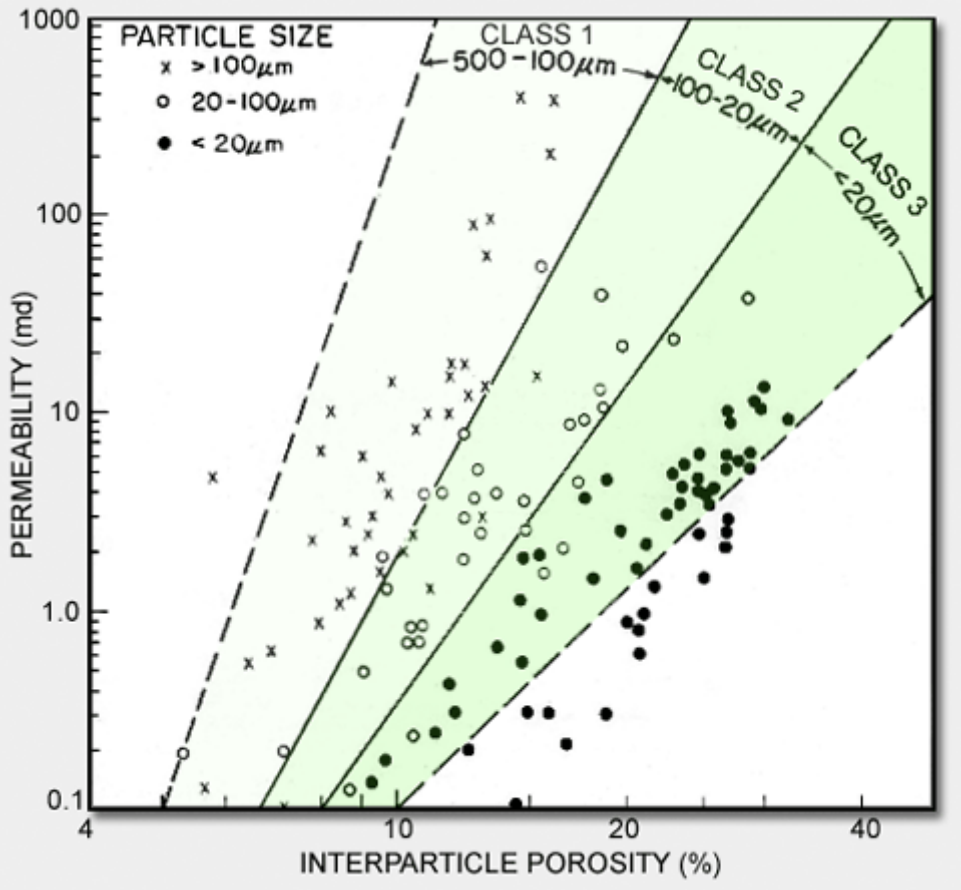

Figure 2.14: Permeability (log-scale) as a function of porosity (aritmetic) and grain size (Lucia, 1995)

In limestone rocks (apart from mudstones), at least two types of porosity affect the petrophysical characteristics, in quite different ways.

• The micro-porosity (micro-connected porosity) always present in the allochems and matrix (mud).

• The macro-connected porosity sometimes found between the allochems (intergranular), and also – rarely – in the dissolution vugs if they are present in sufficient numbers to be interconnected.

Only macro-connected porosity plays a significant role in permeability.

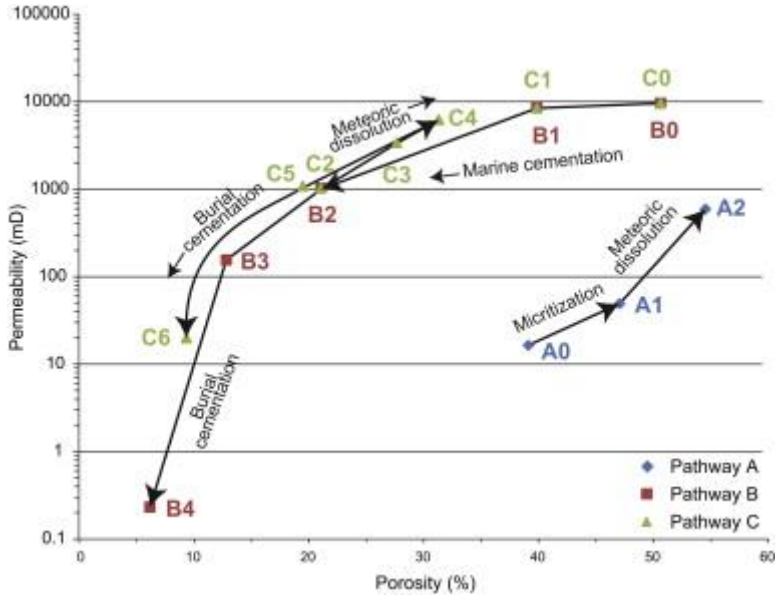

Figure 2.15: Porosity and permeability evolution through different diagenetic environments of the Pore Architecture Models (PAMs) based on synthetic textural images at different stages of carbonate diagenesis. A0, B0 and C0 are the starting (depositional) sediments, subsequent numbers indicate different textures (van der Land et al, 2013).

2.2.3. Mechanical properties of carbonate rocks

Mechanical properties of carbonated rocks may significantly vary depending on composition and weathering. Furthermore, as for all fractured rock masses, mechanical properties are significantly scale-dependent, due to heterogeneity at different scales. Indeed, a fractured rock mass consists of intact rock and discontinuities of different size and spacing: fissures, vugs, single fractures, sets of fractures.

Mechanical properties are usually investigated by laboratory tests, using samples of small dimensions that cannot intercept the fractures, thus are not representative of the in situ behaviour. Moreover, the smaller the specimen, the fewer the discontinuities present and hence a smaller specimen may be expected to have a higher stiffness than a large specimen (Beniawski, 1978).

Figure 2. displays values of Young's modulus collected by Vilarrasa et al (2013) for a great number of carbonated rocks and at different scales (Beniawski, 1978; Ide, 1936; Heuze, 1980; Shalabi et al, 2007). Values are the result of laboratory tests or field tests. The size of the analyzed sample depends on the experimental setting of each study; furthermore, for some materials, stiffness is estimated at different spatial scales. In general, values result extremely different, varying within a range of two orders of magnitude (from 1GPa to almost 100GPa). Nevertheless, it is possible to observe a main trend showing a dependence of the mechanical properties on the scale: stiffness decreases as the scale increases.

Therefore, mechanical characterization of carbonate rocks is very influenced by spatial scale effects. Core sample laboratory tests may overestimate the in situ value of stiffness. Thus, in order to estimate a correct value of Young's modulus, a large scale analysis (field test or back analysis) should be performed as well as to consider the great dimension and spacing of the fractures.

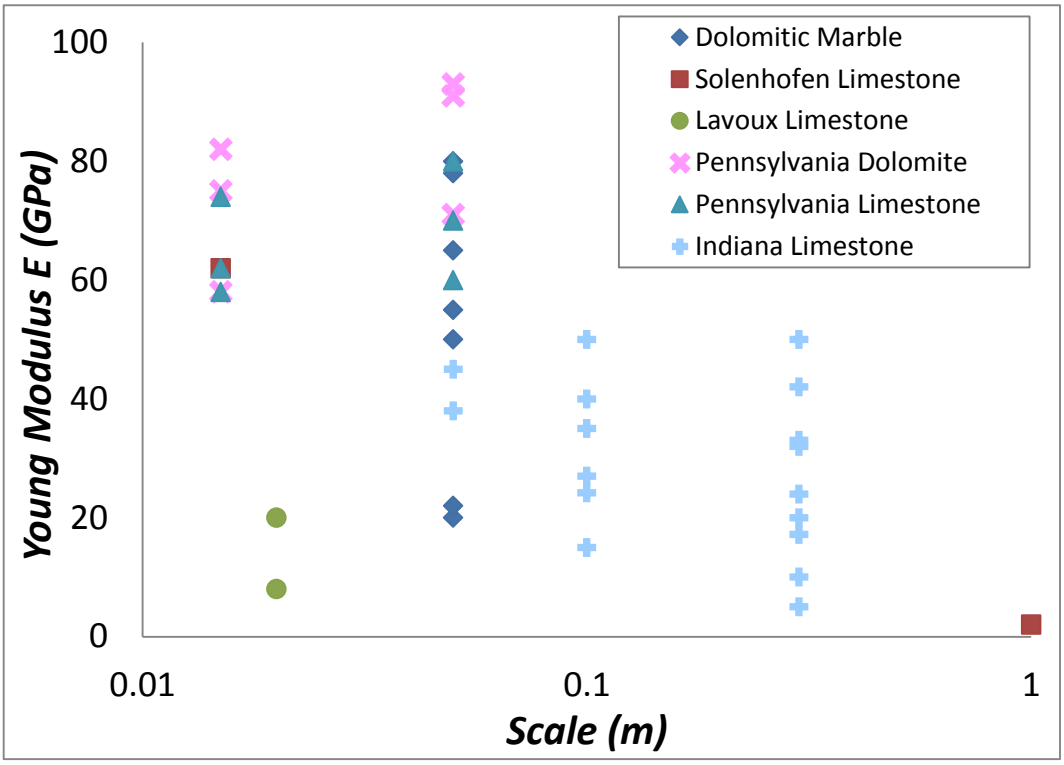

Figure 2.16: Values of Young's modulus for different carbonated rocks and spatial scales. Values are collected from several experimental study (see reference in the text).

2.3. Injection of CO_2 into Carbonates

Hontomin is unique in being proposed as a CO_2 injection site into relatively low permeability carbonate rocks for dedicated geological storage. As shown in Figure 2., the pH of brine in equilibrium with CO_2 drops significantly with increasing pressure of CO_2. That is, the aqueous phase becomes acidified as CO_2 is dissolved (note that dissolved CO_2 concentration grows linearly with CO_2 pressure until the pressure is so high that CO_2 does not behave as an ideal gas). As a result, carbonate is also dissolved, which is apparent in the build-up of the concentration of Ca in the aqueous phase. For every two moles of CO_2 dissolved, approximately one becomes bicarbonate and one mole of calcite is dissolved, which explains why the plots of Ca and bicarbonate in Figure 2.have gradients around half for that of CO_2.

The dissolution of carbonate could theoretically promote pervasive dissolution andcause formation of cavities, which might compromise the stability of the storage formation and caprock. To address this issue:

- Large-scale CO_2 injection in carbonate formations was simulated to understand the overall amount of calcite that can be dissolved, and
- Small scale laboratory experiments were performed, to understand the conditions under which dissolution will form localized wormholes.

Modelling the scenarios, defined in section 3.4, to simulate multiphase flow and reactive transport followed the approach of Saaltink et al. (2013) and included: the displacement of brine by supercritical CO_2 (1,500m depth, 60ºC), the dissolution of CO_2 in the brine and resulting acidification, and the dissolution of calcite. Two cases have been considered for permeability: 100mD, which leads to density dominated flow (i.e., the CO_2 tends to float on top of the brine); and specifically for this study,

10mD, which maintains viscous dominated flow conditions (i.e., cylindrical push away from the injection well) for much longer. These permeabilities were obtained from information previous to the drilling of wells at the Hontomín site, more specifically, acquired from the existing oil wells (H-1 to H-4) located nearby and reaching the reservoir formation. Permeability measurements obtained from injection tests in the Hontomin wells are about 1mD (Ref Report Milestone5 FPA041), that is one or two orders of magnitude lower than the modelled assumptions. For both modelled cases, overall dissolution wa small (porosity increase of less than 2.10^{-4}) and restricted to the outer edge of the CO_2 plume. The conclusion is that the formation of large cavities is unlikely. This finding could be regarded as counter-intuitive but reflects the rapid decline in carbonate dissolution caused by buffering effects.

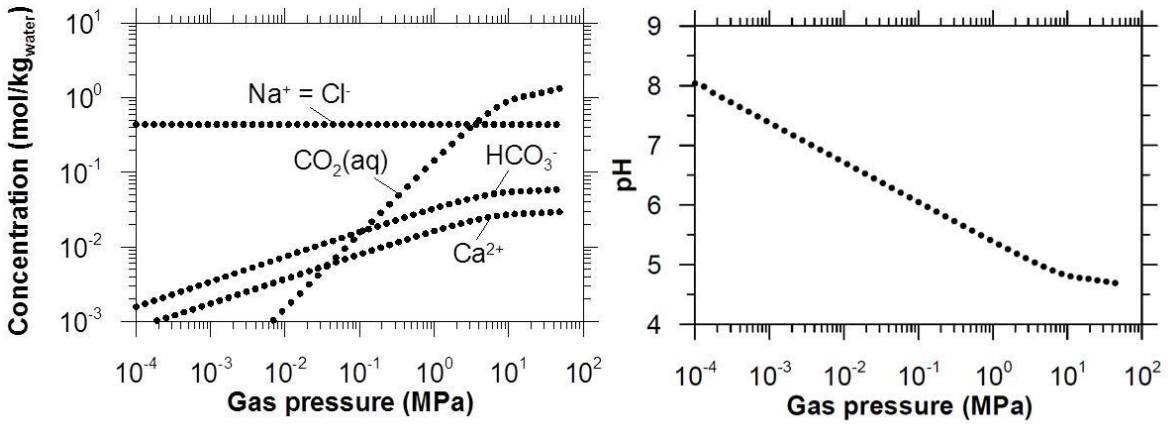

Figure 2.17: Concentrations of the most important species as a function of gas pressure. H_2O-CO_2-Na-Cl-$CaCO_3$ system at 60 ºC.

Insights into the conditions allowing wormhole formation have been gained through laboratory experiments, mostly extracted from the literature but also from specific tests (Luquot and Gouze, 2009; Luquot et al, 2014a, Luquot et al, 2014b). Results from these experiments show that the localization of calcite dissolution depends on the relation between the flux of calcite saturated brine and dissolution rate kinetics. In the two extremes (infinitely fast transport or kinetics), dissolution is homogeneous. However, for a broad range of conditions, dissolution tends to form wormholes. This does not contradict the results of the large scale numerical modelling, because wormhole formation is a small-scale heterogeneous process and a large amount of fluid (thousands of pore volumes) would need to flow through the medium for wormholes to be significant.

3. TESTS TYPES

3.1. PUSH-PULL

3.1.1. Aims and Description

The CO_2 in dense (supercritical or liquid) phase is injected into deep geological formations such as saline aquifers or depleted oil and gas reservoirs. Once injection stops, the supercritical CO_2 plume will migrate laterally and, if the aquifer is inclined, upslope driven by buoyancy (Szulczewski et al, 2012). However, a portion of the CO_2 will lag behind, trapped by capillary forces as a discontinuous phase, in what is termed capillary trapping (Bachu et al, 1994). Estimating the residual CO_2 saturation in a storage formation is important for assessing storage efficiency and long term trapping (Juanes et al, 2006). Unfortunately, direct measurement of residual saturation is not easy; laboratory measurements of residual CO_2 (e.g., Pentland et al, 2011), are problematic and may not be representative of field conditions. Capillary trapping is extremely sensitive to contact angle during CO_2 displacement by brine (or vice versa) and to the heterogeneity of the pore size distribution. Specifically, CO_2 may remain trapped in large pores that are surrounded by much smaller pore necks. This situation is much more frequent in carbonate rocks than other type of rocks. Dissolution tends to occur along elongated channels, wich may trap a large quantity of CO_2 and need to be characterized. Under those conditions, laboratory measurements are not representative and field tests are required. Zhang et al. (2011) proposed such a test, consisting of injecting CO_2 and then displacing it, so that some CO_2 will remain trapped in the formation around the injection well. The question then is how to measure this residual CO_2.

Several geophysical techniques are available to determine CO_2 saturation. Borehole neutron logs measure the hydrogen content in the pore space of the formation and can be used to estimate formation porosity in sedimentary rocks (e.g., Monier-Williams et al, 2009). If water, brine or other fluids are displaced by CO_2 this will change the apparent porosity of the formation. However, the penetration depth of the neutron radiation rarely exceeds 20-30 cm (Serra, 1984), so that only the CO_2 saturation very close to the borehole can be measured. Resistivity logs (e.g., Monier-Williams et al, 2009) and electrical resistivity tomography (ERT; Loke and Barker, 1996; Slichter, 1933) measure the electrical conductance of the porous medium between two electrodes. Conductance depends on the water filled porosity. Unfortunately for typical test conditions, spatial resolution will not be sufficient (the size of the area with residual CO_2 may be of only a few metres). The same is true for seismic methods.

Given the practical difficulties of traditional methods, Zhang et al. (2011) proposed combining three sets of tests: thermal, tracer and hydraulic.

- Thermal tests consist of installing a Distributed Temperature Perturbation Sensing (DTPS, Freifeld et al, 2008) along CO_2 injection and observation wells (Freifeld et al, 2009). For DTPS, a fibre-optic distributed temperature sensor (DTS) is deployed in a borehole along with a heater cable. The formation is heated and the rate of temperature increase is measured using the DTPS. DTPS measures the thermal diffusivity of the porous medium to detect the presence of CO_2 in the pore space. The degree of CO_2 saturation affects the thermal conductivity and to a lesser extent the heat capacity of the formation, which changes the rate of temperature increase upon heating. The depth of penetration of the thermal front into a formation with typical thermal properties after 2 days of heating at 40W/m is about 1–2m (Zhang et al, 2011). However, the sensitivity of DTPS to CO_2 saturation may be low (Zhang et al, 2011). Particularly, in formations with low porosity, like Hontomin, the change of the bulk thermal properties of the formation with/without the presence of CO_2 is small, and if the power

of the heater is low, then tests need to be very long (up to a week) to obtain changes in thermal response above the DTS measurement accuracy (Cubillo et al, 2012).

- Tracer tests consist of injecting water with a partitioning tracer, highly soluble in CO_2, and then pumping it back. The difference between the injected and extracted tracer concentration reflects the amount that has been dissolved in the CO_2, which is proportional to CO_2 saturation. The test is elegant and potentially accurate, but extremely difficult to carry out, because a large volume of CO_2 saturated brine needs to be injected. Moreover, given the limited transport distance, it is hard to ensure that the injected tracer equilibrates with the CO_2.

- Hydraulic tests consist of imposing a pressure perturbation (for example by pumping or injecting water) on a porous medium and measuring the pressure response to infer its transmissivity and storage coefficient. Both parameters change due to the presence of CO_2 in the pore space.

Hydraulic tests are performed routinely in hydrogeology and petroleum engineering to obtain information on the hydraulic parameters of the well and the formation. Particular phenomena such as wellbore storage, skin effects (i.e. a zone with permeability usually lower than that of the formation in the casing or in a region close to the wellbore) and different formation boundary conditions each have a characteristic effect on the shape of the observed pressure response (or so-called drawdown curve). Therefore, significant information about the residual CO_2 can be drawn from a detailed analysis of the wellbore response to a hydraulic test.

3.1.2. Operational conditions

The proposed test consists of the following steps:

i. Perform conventional hydraulic tests to measure initial formation parameters and decide the lowest possible flow rate with a measurable response (about 1,000 times the resolution of pressure sensors).
ii. Start CO_2 push-pull test by injecting CO_2 with tracers: some 100 - 200t CO_2 in the Hontomin case
iii. Shut in period
iv. Create the residual CO_2 zone around the well. This can be accomplished in two ways (Zhang et al, 2011): either by producing CO_2 and brine until all mobile CO_2 is extracted and only residual and therefore immobile CO_2 is present in the aquifer, or by injecting CO_2-saturated brine to push all mobile CO_2 further into the formation and leave only residual CO_2 behind. While Zhang et al. (2011) prefer the second approach; here we opt for the first approach because back-production (i.e. extraction of the injected CO_2) limits the final width of the CO_2 zone, which is necessary to keep the total duration of the hydraulic tests short. We expect CO_2 dissolution to be small because the surrounding brine will be CO_2 saturated.
v. Perform post-injection hydraulic test with the same conditions as in step (i) but by injecting CO_2 saturated brine at a low flow rate to avoid dissolution or displacement of residual CO_2

In order to avoid large values of wellbore storage that could mask changes in the hydraulic parameters close to the well, the test will be performed in pressurized mode. To this end, prior to the test the down-hole valve of the injection well will be closed, and the injection pipe will be completely filled with water up to the pump. At the beginning of the test, either the pump will have to be started and the valve will have to be opened simultaneously, or preferably (if no damage to the equipment is to be expected) the pump should work for a short time against the closed down-hole valve, and then the valve should be opened to start the injection. Besides down-hole pressure data, the flowrate in the injection pipe should be recorded precisely and with a high sampling frequency, especially during the first minutes of the test. It has to be kept in mind that results will be evaluated against the logarithm of

time. Therefore, a high (initial) sampling frequency is required to derive parameters in and close to the well from the obtained data.

During CO_2 extraction (step iv) the gas volume and composition should be measured using a phase separator and a gas analysis system, and the concentration of CO_2 dissolved in the extracted brine should also be determined at short time intervals on-site (e.g. by measuring pH and alkalinity, or by Raman spectroscopy). Extraction should be stopped when the total mass of CO_2 (gaseous + dissolved) per volume of extracted brine is equal to the equilibrium concentration of dissolved CO_2 at down-hole pressure and temperature conditions, in order to avoid excessive re-dissolution of residual CO_2 by fresh brine flowing towards the CO_2 zone.

More information on the influence of CO_2 on hydraulic parameters and test modeling results have been published in Martinez-Landa et al, (2013).

3.2. SUPERCRITICAL INJECTION

3.2.1. Aims and Description

This test simulates the 'traditional' option for CO_2 storage - injecting a continuous flux of CO_2 as a surface gas (for example, 50 bars and 20°C) would be enough to reach the reservoir downhole in a supercritical state.

The pressure (P) and temperature (T) conditions of deep geological formations suitable for storing carbon dioxide (CO_2) are such that this greenhouse gas remains in supercritical (SC) state, i.e. P>73.82 bar and T>31.04 ºC (e.g. Bachu, 2003). Thus, it is usually assumed that CO_2 will reach the aquifer in SC conditions (e.g. Pruess and Garcia, 2002). However, inflowing CO_2 does not need to be in thermal equilibrium with the aquifer

The objective of this injection test is multiple. On one hand, to verify the correct operation of the injection system and, where necessary, to make changes. On the other, it is the reference test for all tests and injection strategies to be performed later. To this end, we present here the evolution of the plume shape and bottomhole pressure for several values of permeability (the full set of properties are displayed in Table 3.1.

3.2.2. Shape and size of the plume and CO_2 pressure

The injection of supercritical CO_2 in deep saline aquifers leads to the formation of a CO_2 plume that tends to float above the formation brine. As pressure builds up, CO_2 properties including density and viscosity can vary significantly. Buoyancy effects are relevant in the CO_2 plume evolution regardless of the injection conditions because the CO_2 is less dense than the brine, but gravity forces gain strength in the case of supercritical CO_2 injection.

To quantify the relative influence of buoyancy we define a gravity number, Ng, as the ratio of gravity to viscous forces. Large values of the gravity number (Ng >> 1) indicate that buoyancy forces dominate. On the other hand, small gravity numbers (Ng << 1) indicate that viscous forces dominate. Note that buoyancy forces will always dominate far from the injection well whereas the opposite is generally true near the well (Vilarrasa et al, 2010).

Table 3.1 Material properties used in the analysis of supercritical CO_2 injection.

Property	**Value**
Permeability, k (m^2)	$2{\cdot}10^{-15}$, $6{\cdot}10^{-15}$, $1{\cdot}10^{-14}$, $5{\cdot}10^{-14}$, $1{\cdot}10^{-13}$
Gas entry pressure, P_{cc} (bar)	0.2
Porosity (-)	0.01

Young's modulus, E (GPa)	30
Poisson ratio, υ (-)	0.3
Temperature, T (K)	315
Depth, d (m)	1500
Thickness, b (m)	130
Brine density, ρ_w (Kg/m^3)	1030
Reference pressure, P_0 (bar)	150
CO_2 density for the reference pressure, ρ_c (Kg/m^3)	766.5
CO_2 mass flow rate, Q_m (Kg /s)	1
Well radius, r (m)	0.07

To find the interface position we use two solutions: a semi-analytical solution for compressible CO_2 injection (Vilarrasa et al, 2013); and a correction to account for CO_2 compressibility (density variations) and viscosity variations (Vilarrasa et al, 2010) using the analytical solutions of Nordbotten et al. (2005) and Dentz and Tartakovsky (2009). The latter are somewhat standard, while the former allows accounting for the plume evolution more accurately even in cases where the plume does not reach the bottom of the formation.

(a)

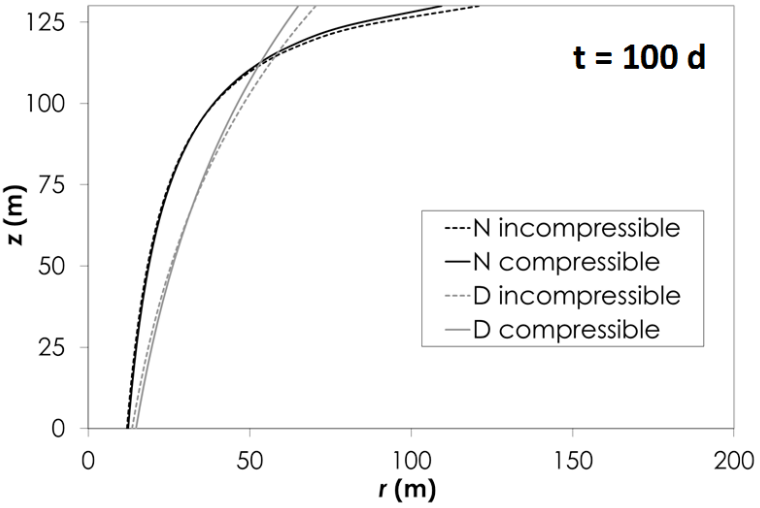

(b)

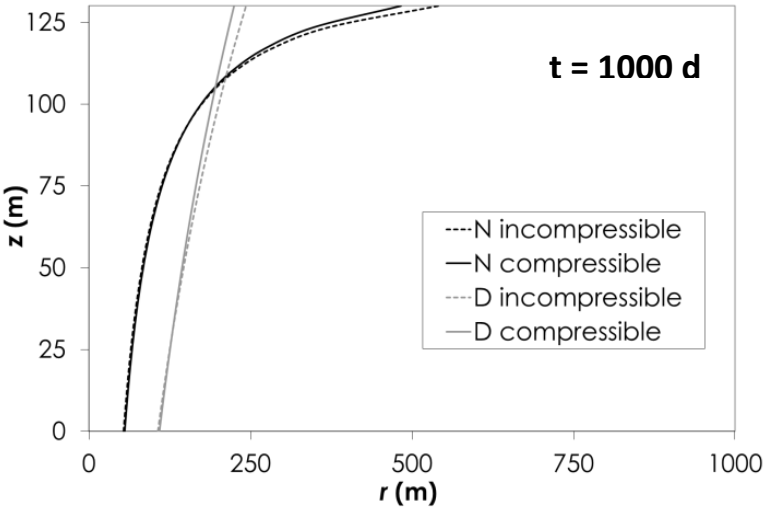

Figure 3.1: Model on plume position aftert 100 and 1000 days. Z(m) represents the thickness of the aquifer and r(m) the distance from the well wall. The injection takes place though the whole thickness of the aquifer (130m). (a) CO_2 plume shape after 100 days and (b) 1000 days of injecting supercritical CO_2 using the analytical solutions of Dentz (D) and Nordbotten (N) and the correction of Vilarrasa to account for CO_2 compressibility with a permeability of $2 \cdot 10^{-15}$ m^2.

We first present results using the correction of Vilarrasa to account for CO_2 compressibility, which assumes that injection takes place through the whole thickness of the aquifer. Figure 3.1 displays the plume position with a permeability of $2 \cdot 10^{-15} m^2$ after 100 and 1000 days of supercritical CO_2 injection. Notice that compressibility does not appear to be a critical parameter in this case, but the solutions of Nordbotten et al. (2005) and Dentz and Tartakovsky (2009) are quite different. Under the test conditions (low permeability, which implies high viscous resistance to flow), the solution of Nordbotten should be better (Vilarrasa et al, 2010).

The semi-analytical solution considers that CO_2 injection is only performed at the top of the formation (i.e., CO_2 is not injected through the whole thickness) and gives good estimates regardless of the gravity number. Figure 3.2 shows the plume position at different times using this solution with a permeability of $2 \cdot 10^{-15}$ m^2.

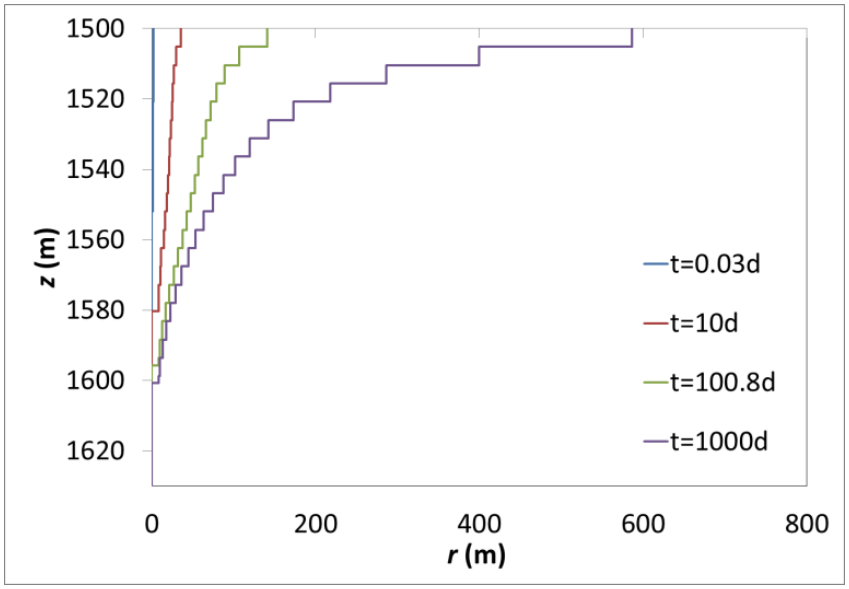

Figure 3.2: Model on plume position at different time. Z(m) represents the depth of the aquifer and r(m) the distance from the well wall. The injection takes place in the upper part of the aquifer (point at the 1500m depth). CO_2 plume at different times with a permeability of $2 \cdot 10^{-15}$ m^2 after injecting supercritical CO_2 using the semi-analytical solution.

Figure 3.2 is somewhat surprising in that the plume (t= 1000d) does not reach the formation bottom and (100d) does not quite look as the N solution in Figure 4.1. To gain some insight, we compute the gravity number.

The gravity number near the well (at a radius of 1m) is about 2.10^{-1}, so gravity and viscous forces are comparable. Therefore, the interface position is similar to the solution of Nordbotten et al. (2005) in the lower half of the aquifer, where viscous forces may dominate, but is similar to that of Dentz and Tartakovsky (2009) in the upper part of the aquifer, where buoyancy begins to dominate.

The error associated with neglecting compressibility increases when gravity forces dominate, which is likely to occur at late injection times.

Table 3.2: Gravity number at a radial distance of 1 m for several values of permeability.

Permeability(k) (m^2)	Permeability (mD)	Gravity number (Ng)	Dominant forces (gravity or viscous forces)
$6 \cdot 10^{-15}$	5.8	0.61	Comparable
$1 \cdot 10^{-14}$	9.8	1.0	Comparable
$5 \cdot 10^{-14}$	49	5.1	Gravity forces
$1 \cdot 10^{-13}$	98	10.25	Gravity forces

A sensitivity analysis was performed with permeability values of 6.10^{-15}, 1.10^{-14}, 5.10^{-14} and 1.10^{-13}, to compare the influence of gravity and viscous forces using the semi-analytical solution. The higher the permeability, the greater the gravity number (Table 3.2) and the relevance of buoyancy forces dominate over the viscous forces as in Figure 3.3, Figure 3.4, Figure 3.5 and Figure 3.6. Notice that as permeability increases, the injection depth is reduced whereas the plume radius is increased.

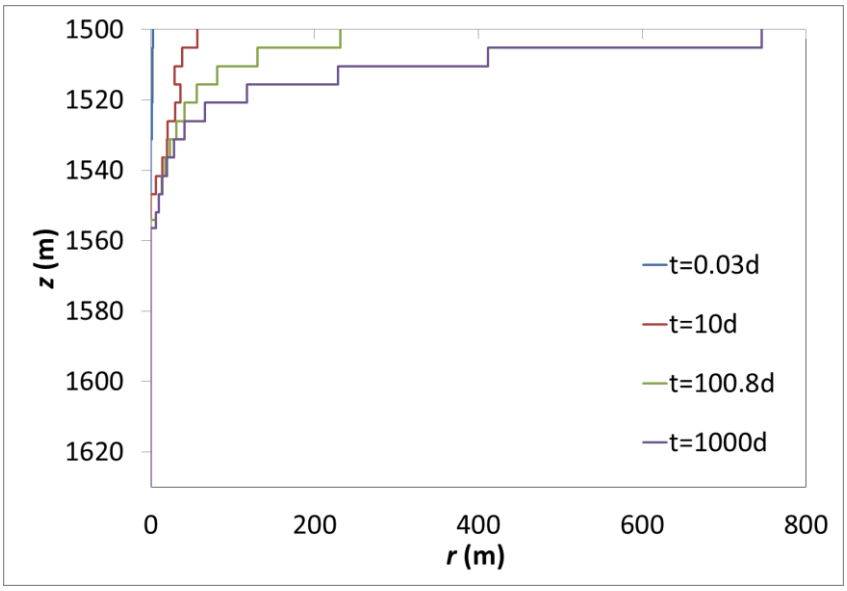

Figure 3.3: CO_2 plume at different times with a permeability of $6 \cdot 10^{-15}$ m^2 after injecting supercritical CO_2 using the semi-analytical solution. Z(m) represents the depth of the aquifer and r(m) the distance from the well wall. The injection takes place in the upper part of the aquifer (point at the 1500m depth).

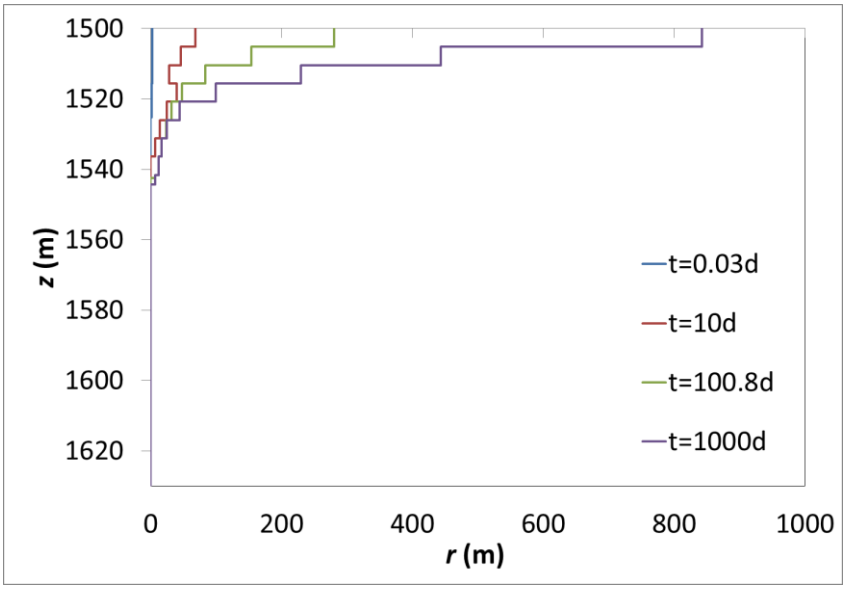

Figure 3.4: CO_2 plume at different times with a permeability of $1 \cdot 10^{-14}$ m^2 after injecting supercritical CO_2 using the semi-analytical solution. Z(m) represents the depth of the aquifer and r(m) the distance from the well wall. The injection takes place in the upper part of the aquifer (point at the 1500m depth).

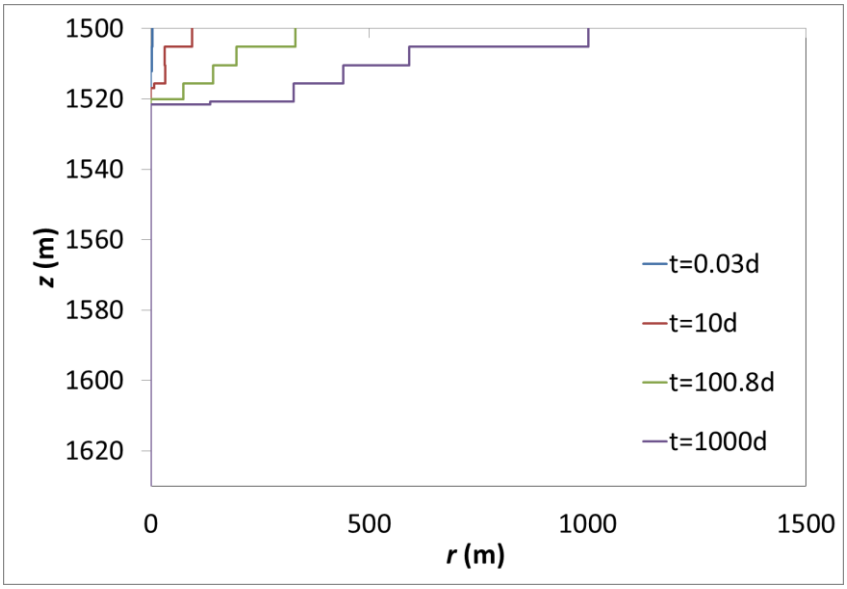

Figure 3.5: CO_2 plume at different times with a permeability of $5 \cdot 10^{-14}$ m^2 after injecting supercritical CO_2 using the semi-analytical solution. Z(m) represents the depth of the aquifer and r(m) the distance from the well wall. The injection takes place in the upper part of the aquifer (point at the 1500m depth).

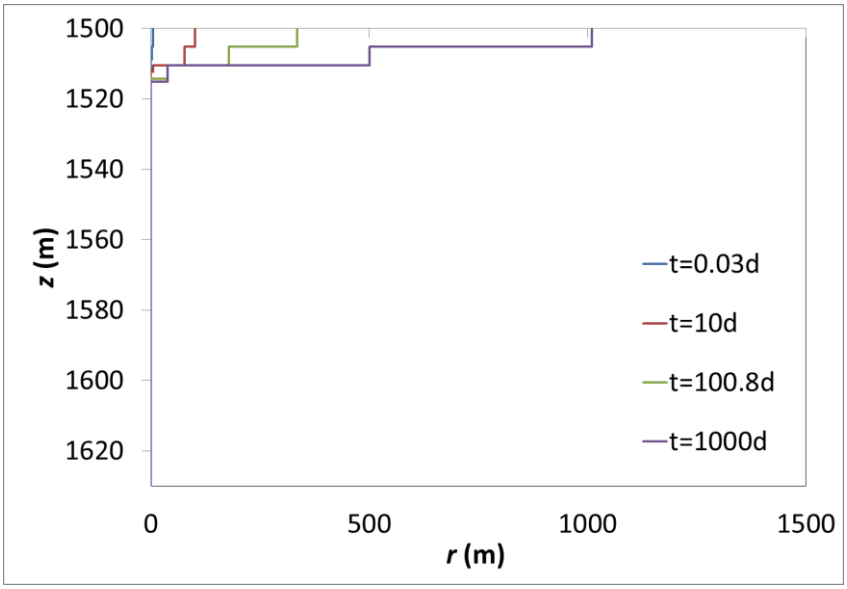

Figure 3.6: CO_2 plume at different times with a permeability of $1 \cdot 10^{-13}$ m^2 after injecting supercritical CO_2 using the semi-analytical solution. Z(m) represents the depth of the aquifer and r(m) the distance from the well wall. The injection takes place in the upper part of the aquifer (point at the 1500m depth).

Pressure evolution

In addition to the evolution of the CO_2 plume, it is important to understand the evolution of pressure changes. Pressure affects the required compression energy, CO_2 density and the mechanical stability of the caprock (Rutqvist et al. 2007; Ferronato et al. 2010; Vilarrasa et al. 2012). Furthermore, the CO_2 plume thickness at the injection well progressively increases with time as CO_2 pressure builds up.

Figure 3.7 displays the vertically averaged fluid overpressure as a function of the logarithm of distance to the well after (a) 100 days and (b) 1000 days of injection using the method of Vilarrasa et al. (2010) to account for CO_2 compressibility in the analytical solutions of Nordbotten (2005) and Dentz and Tartakovsky (2009), with a permeability of 2.10^{-15} m^2. Pressure at the bottom of the aquifer is approximately 17 MPa in both cases. The first change in slope beginning from the right hand side of the figure indicates the CO_2-brine interface position in each case.

The higher the permeability, the lower the overpressure as shown in Figure 3.8, Figure 3.9, Figure 3.10 and Figure 3.11.

(a)

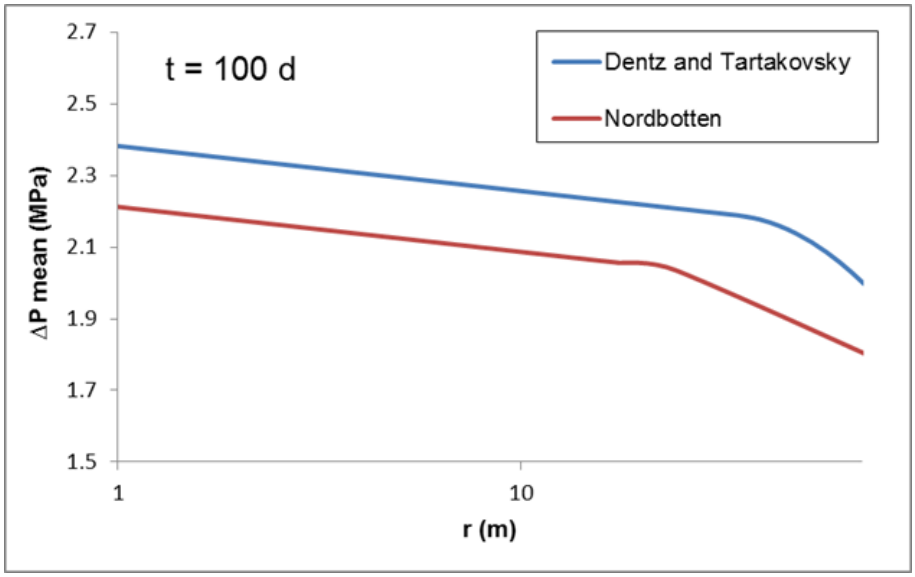

(b)

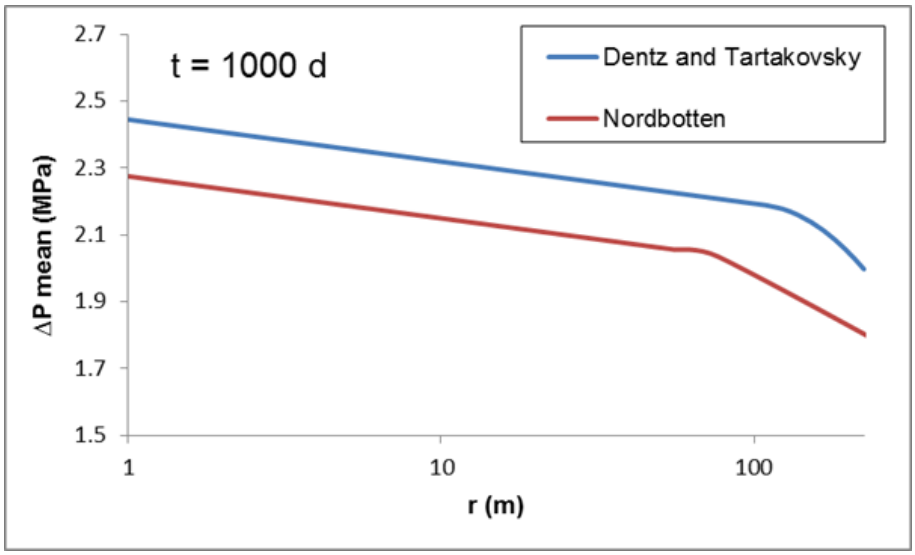

Figure 3.7: Vertically averaged fluid overpressure as a function of the logarithm of distance to the well after (a) 100 days and (b) 1000 days of injection with a permeability of 2.10^{-15} m^2.

CO_2 pressure at the top of the aquifer is lower than the vertically averaged fluid pressure, which considers CO_2 and the formation brine. The relationship between pressure and density is in general non-linear. Moreover, pressure varies in space. Notice in Figures 4.7-4.11 that the dependence is two-way: CO_2 density depends explicitly on fluid pressure, but fluid pressure also depends on density as this controls the plume volume and thus the fluid pressure through the volume of water that needs to be displaced.

(a)

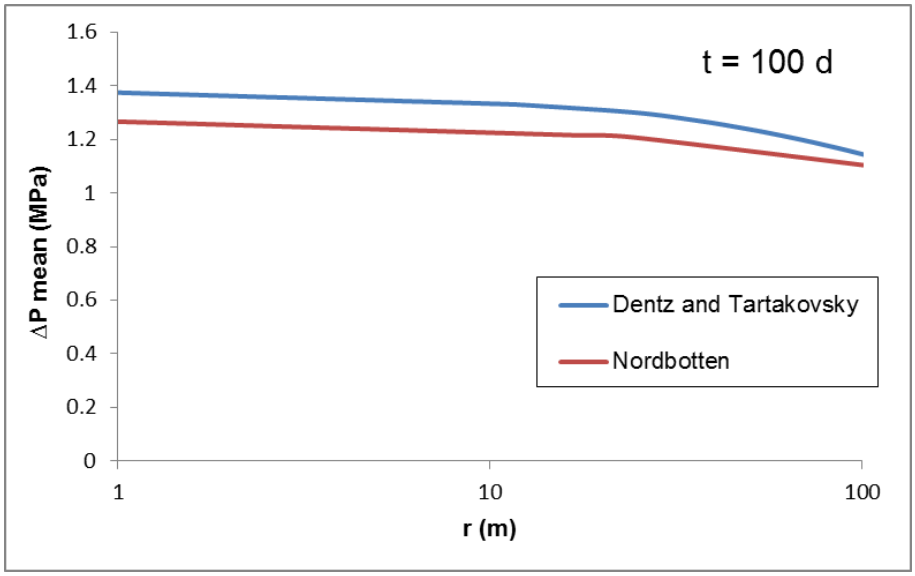

(b)

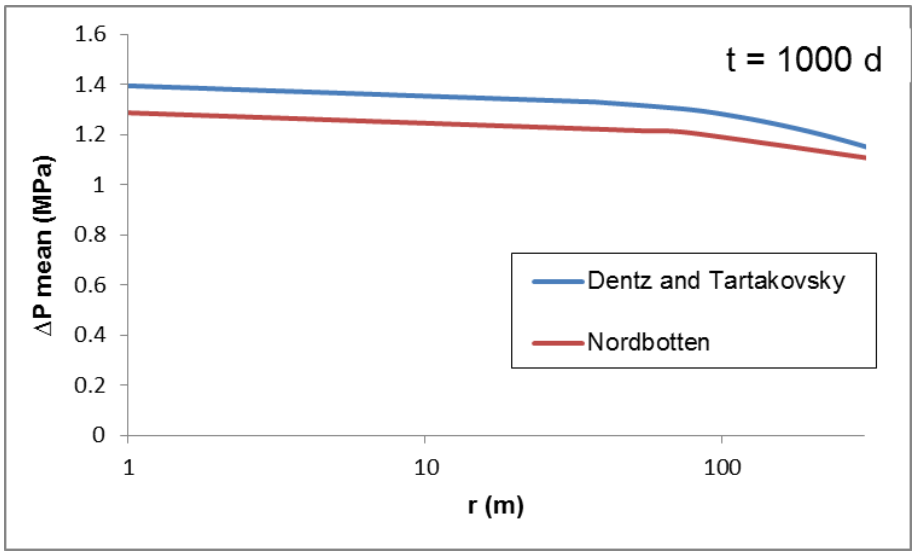

Figure 3.8: Vertically averaged fluid overpressure as a function of the logarithm of distance to the well after (a) 100 days and (b) 1000 days of injection with a permeability of $6 \cdot 10^{-15}$ m^2.

(a)

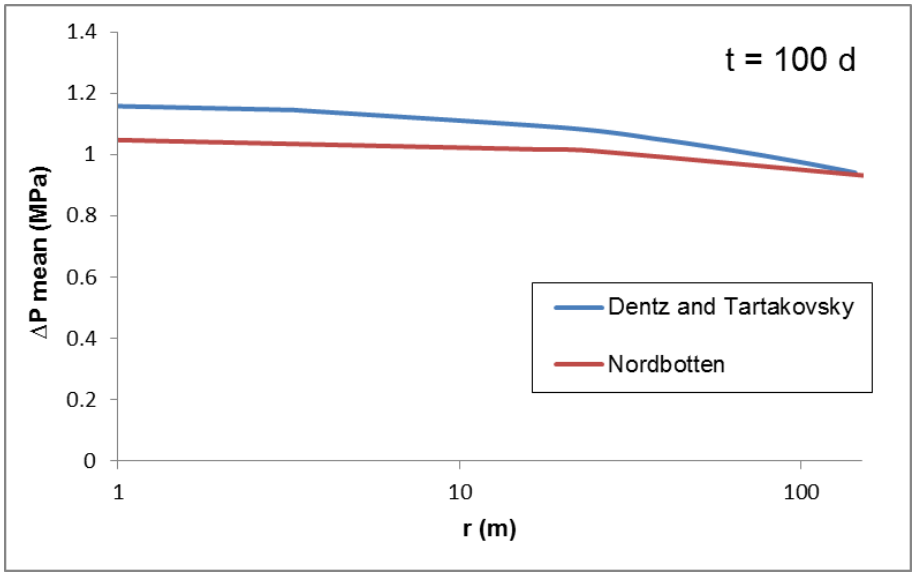

(b)

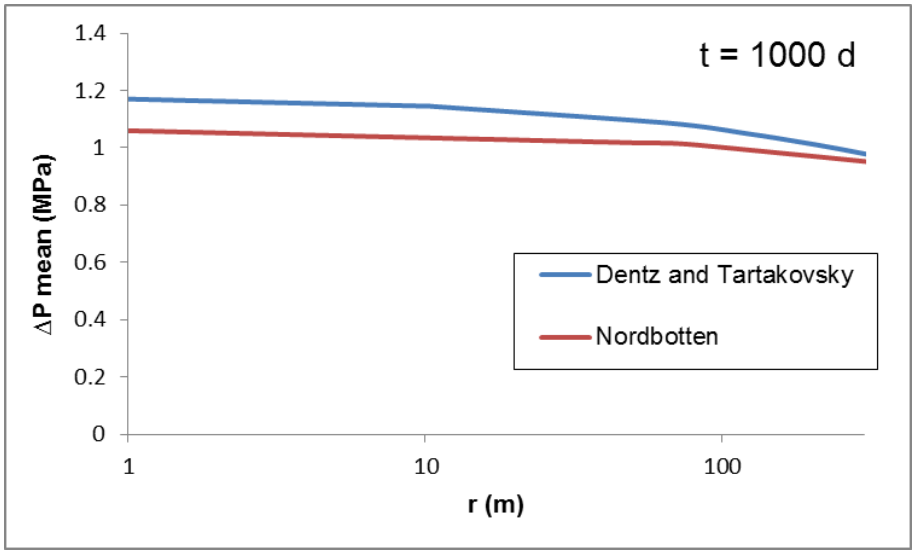

Figure 3.9: Vertically averaged fluid overpressure as a function of the logarithm of distance to the well after (a) 100 days and (b) 1000 days of injection with a permeability of $1 \cdot 10^{-14}$ m^2.

(a)

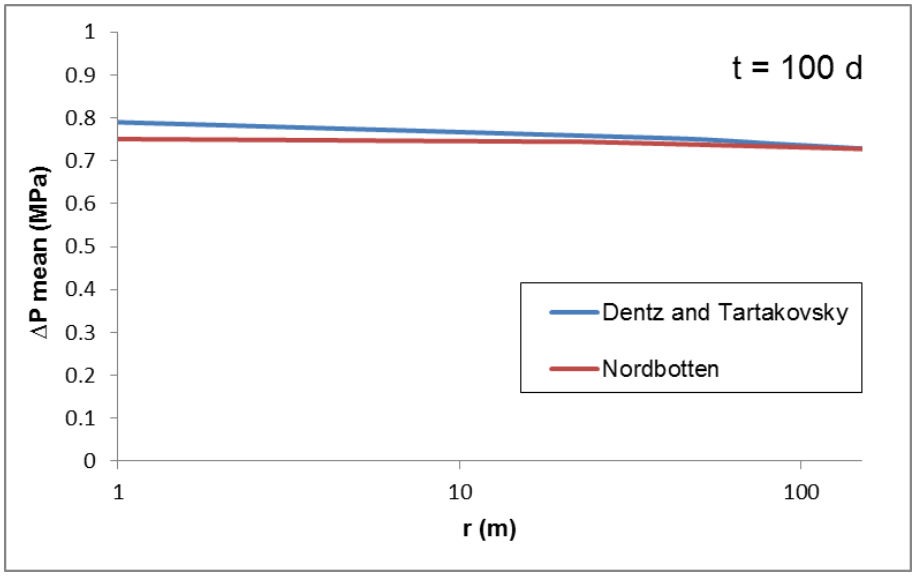

(b)

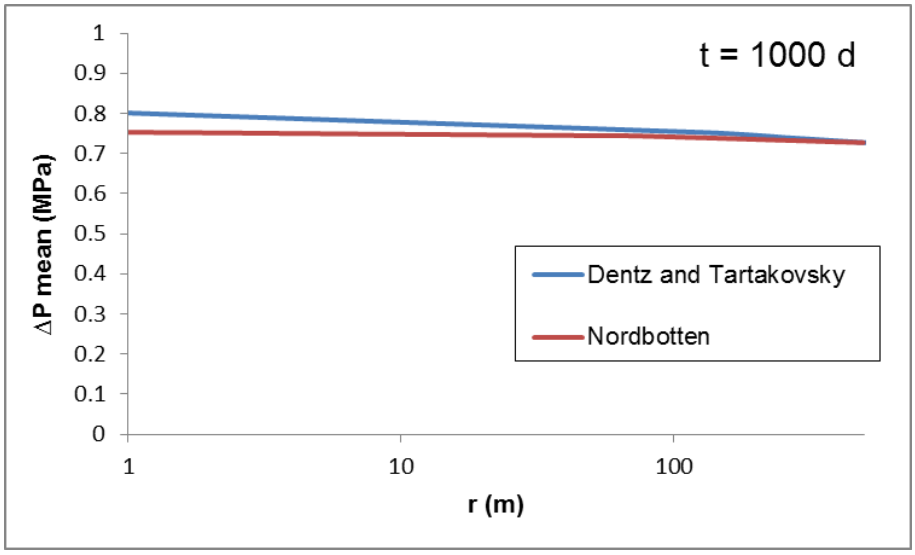

Figure 3.10: Vertically averaged fluid overpressure as a function of the logarithm of distance to the well after (a) 100 days and (b) 1000 days of injection with a permeability of $5 \cdot 10^{-14}$ m^2.

(a)

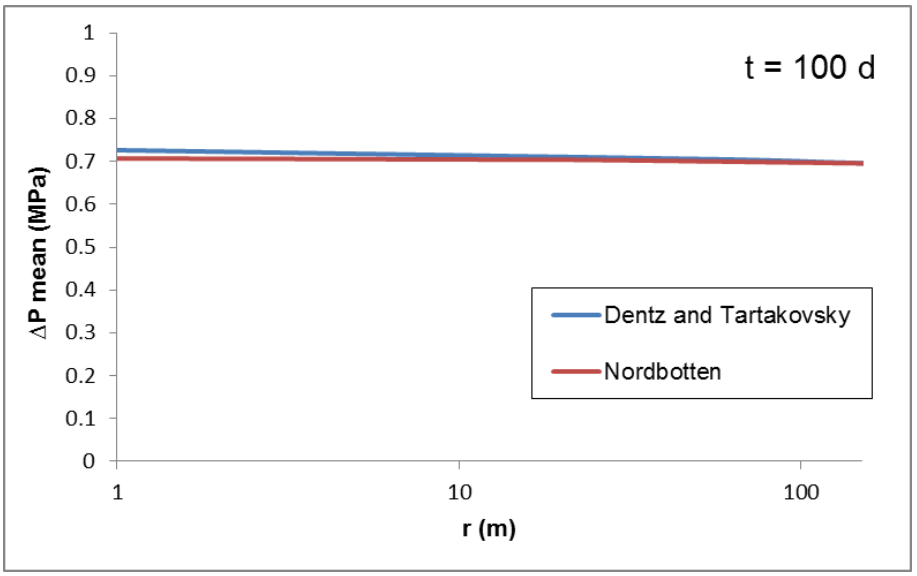

(b)

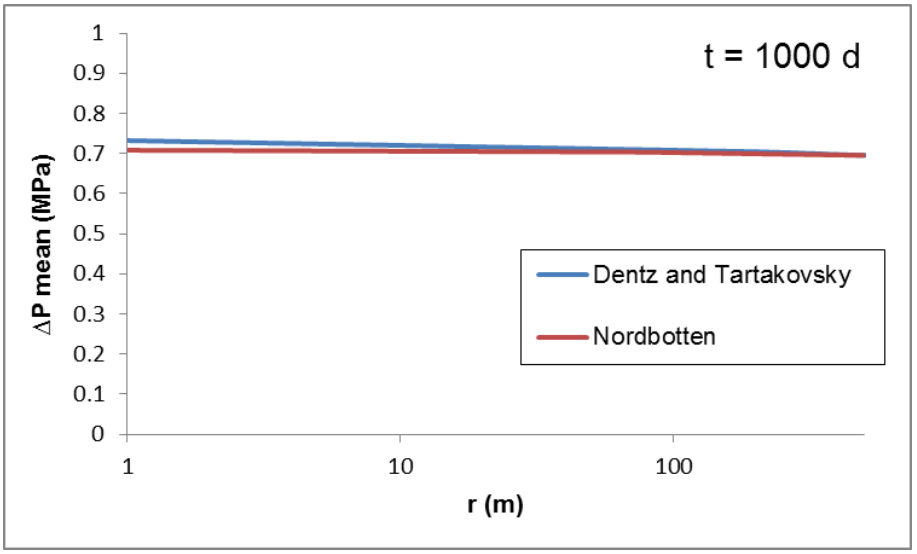

Figure 3.11: Vertically averaged fluid overpressure as a function of the logarithm of distance to the well after (a) 100 days and (b) 1000 days of injection with a permeability of $1 \cdot 10^{-13}$ m^2.

Both analytical solutions, i.e. Nordbotten et al. (2005) and Dentz and Tartakovsky (2009), describe similar behaviour, but Nordbotten et al. (2005) gives rise to greater errors. This is mainly because vertical fluid pressure is averaged, which leads to unrealistic CO_2 properties in the zone where both CO_2 and brine exist. For gravity numbers greater than 1, the mean CO_2 density tends to a constant value because fluid pressure build up in the well is very small. For this reason, the relative error remains constant for this range of gravity numbers (Vilarrasa et al, 2010).

3.2.3. Operational conditions and test procedure

Injection of CO_2 as a gas at the surface (e.g. 50 bar and 20 ºC) may be sufficient to result in supercritical CO_2 downhole. However, the set of processes involved are highly complex.

Injection of a consistent and sufficient flow rate into the well ensures that CO_2 is maintained in supercritical conditions below fracture pressures, and avoids 'push back' from other wells. Subject to the depth at which an aquifer is located and assuming near hydrostatic conditions, the supercritical phase can be verified without difficulty (CO_2 conditions at the wellhead are discussed in section 4.3).

Ideally, the duration of the test should be long enough to activate dissolution of CO_2 at the bottom of the plume. However, this might take too long because permeability at Hontomín is very low. Based on the equations of Hidalgo and Carrera (2009), the test duration would be several years. Therefore, the actual duration will be conditioned by other factors (e.g. availability of CO_2). CO_2 dissolution could be activated by intermittent injection (see section 4.4).

The control parameters during the test are:

- Fluid pressure and temperature at injection (HI) and observation (H-A) well.

- Rate of injection.

3.3. LIQUID CO_2 INJECTION

3.3.1. Aims and Description

Suitable reservoirs for storing CO_2 should have pressure and temperature conditions which ensure that CO_2 will remain in a supercritical state to provide efficient storage. However, injecting relatively cold CO_2 may lead to a region around the injection well where CO_2 stays in a liquid state. Further away, CO_2 equilibrates with reservoir temperatures, leading to supercritical CO_2 conditions.

It could be inferred that injecting CO_2 in a liquid state is more energy-efficient than doing so in an SC state and may optimize storage efficiency due to a higher density. Therefore any given mass of CO_2 injection as a liquid will displace a smaller volume of formation fluid, leading to a lower overpressure in the reservoir. More importantly, the increased weight of liquid CO_2 in the injection well implies that a significantly lower pressure is required at the wellhead. Additionally, CO_2 is usually transported in liquid state (pressure above 8.5 MPa and ambient temperatures). Thus it can be injected at the conditions in which it arrives at the wellhead, without having to perform throttling or heating operations. Reduced pressure at the wellhead may be lower than transport pressure and therefore allow recovery of some energy from the incoming CO_2. Furthermore, if pressure needs to be increased for injection less compression has to undertaken due to the lower compressibility compared to SC CO_2. This level of compression could be performed by means of pumps without compressors, thus easing operations (Vilarrasa et al, 2014).

Despite all these potential advantages, cooling the reservoir around the injection well will cause a thermal stress reduction (Segall and Fitzgerald, 1998) that might induce fracture instability and microseismic events (Vilarrasa et al, 2014). Microseismic events may open or widen fractures and therefore increase permeability; however, such events could also cause mechanical instability of the caprock and therefore increase risks associated with CO_2 leakage.

These thermo-mechanical effects have been widely studied in the field of enhanced geothermal systems, where large temperature contrasts occur (e.g. Ghassemi et al, 2007; Koh et al, 2011; De Simone et al, 2013; Rutqvist et al, 2013a). However, most mechanical studies in geologic carbon storage applications concentrate on hydro-mechanical effects and neglect thermal effects (e.g. Bao et al,2013a, 2013b; Yamamoto et al, 2013; Kano et al, 2013; Rutqvistet al, 2013b). However, since liquid CO_2 is colder than the formations where it will be injected, liquid CO_2 injection implies a combination of

hydro-mechanical and thermo-mechanical effects that should be studied simultaneously to properly evaluate caprock mechanical stability (Vilarrasa et al, 2014).

The objective of this assessment is to analyse liquid CO_2 injection into a deep formation in terms of minimizing energy costs and phase changes in the capture–transport–injection chain, and improving short and long-term storage efficiency. Studying the mechanical response of the formation is another objective of the test.

3.3.2. Shape and size of the plume, CO_2 pressure (evolution)

The results presented in this section were obtained from simulations using CODE-BRIGHT (Vilarrasa et al, 2013) where the initial conditions of the injection in the deep saline formation are those at the Hontomín test site: hydrostatic pressure; temperature following a geothermal gradient of 0.033ºC/m, with a surface temperature of 5ºC; a vertical stress gradient of 0.023MPa/m. The geological indicators indicate a normal faulting stress regime. The hydraulic boundary conditions are a prescribed CO_2 mass flow rate at the injection well (1.0Mt/yr), a constant pressure on the outer boundary and no flow at the top and bottom boundaries.

To assess the impact of rock stiffness on responses to temperature changes, the case of a relatively stiff reservoir and caprock have been considered.

The assumed boundary conditions are constant temperature at the upper and lower boundaries of the domain. Neither pressure nor thermal perturbations reach these boundaries, so the nature of these boundary conditions does not affect the results. The mechanical boundary conditions lead to no displacement normal to the bottom, (left and right hand side) and injection well boundaries. A constant, vertical lithostatic stress was assumed at the top of the caprock (Vilarrasa et al, 2013).

Since liquid CO_2 is denser and more viscous than SC CO_2, gravitational forces become less significant than viscous forces, causing a steep CO_2 brine interface close to the injection well (Figure 3.12), where CO_2 remains in liquid state (Figure 3.13). Further away, where CO_2 reaches SC conditions, the CO_2 plume evolution is characterized by gravity override (Nordbotten et al, 2005; Dentz and Tartakovsky, 2009; Vilarrasa et al, 2010) (Figure 3.12).

As can be seen from the simulations, the thermal transition is relatively abrupt (Figure 3.14). CO_2 remains in liquid state close to the injection well, leading to a steep front because viscous forces dominate gravity forces. Once the CO_2 thermally equilibrates with the medium (in a sharp front), CO_2 stays in supercritical state, leading to a CO_2 plume interface dominated by gravity forces. Injection of liquid CO_2 forms a cold region close to the well, which advances far behind the CO_2 plume interface with brine. This leads to a steep liquid CO_2 front (where viscous forces dominate gravity forces) that advances behind the typical CO_2 plume interface (where gravity forces dominate viscous forces). It is observed that the initial (less than 1 year) cooling front is sub-vertical (Vilarrasa et al, 2013), but later expands horizontally and follows the shape of the CO_2 plume. CO_2 remains in a liquid state within the cold region, leading to a significantly higher density (around 900 kg/m3) compared with the rest of the CO_2 plume (around 650 kg/m3), where CO_2 stays in supercritical state.

Temperature distribution within the CO_2 plume is not only affected by the cold CO_2 injection - other processes must be taken into account. There is an interaction between: (1) the warmer CO_2 placed at the bottom of the aquifer, which flows upwards along the interface, (2) the colder brine placed at the top of the aquifer, which flows downwards along the interface, (3) CO_2, which cools with migration away from the injection well due to the Joule–Thomson effect and (4) temperature increases due to the exothermal reaction of CO_2 dissolution into the brine. The net result of these processes is a slight temperature increase in the SC CO_2 region (Figure 3.14).

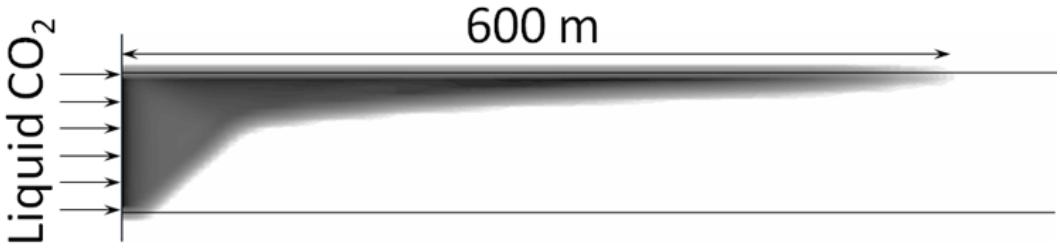

Figure 3.12: CO_2 plume after 1 year injecting 1 MT /yr of CO_2 in liquid state

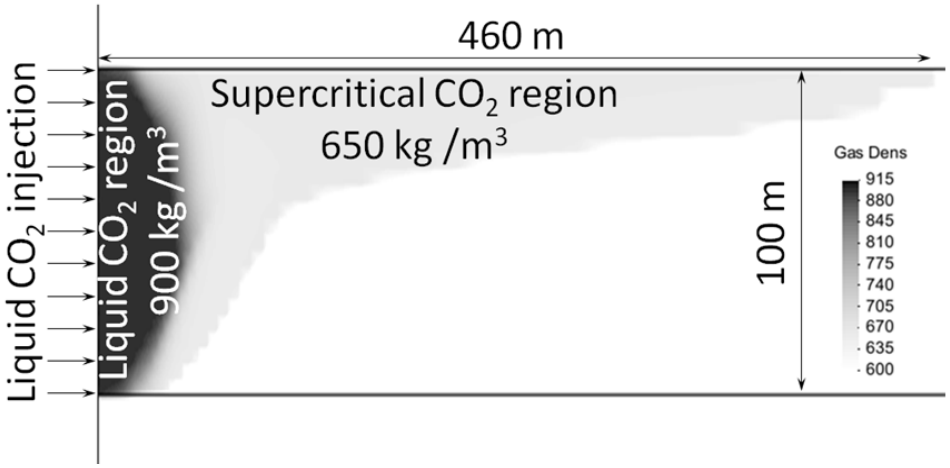

Figure 3.13: CO_2 density after 8 months of liquid CO_2 injection. CO_2 remains in liquid state close to the injection well, leading to a steep front because viscous forces dominate gravity forces. Once the CO_2 thermally equilibrates with the medium (in a sharp front), CO_2 stays in SC state, leading to a CO_2 plume interface dominated by gravity forces.

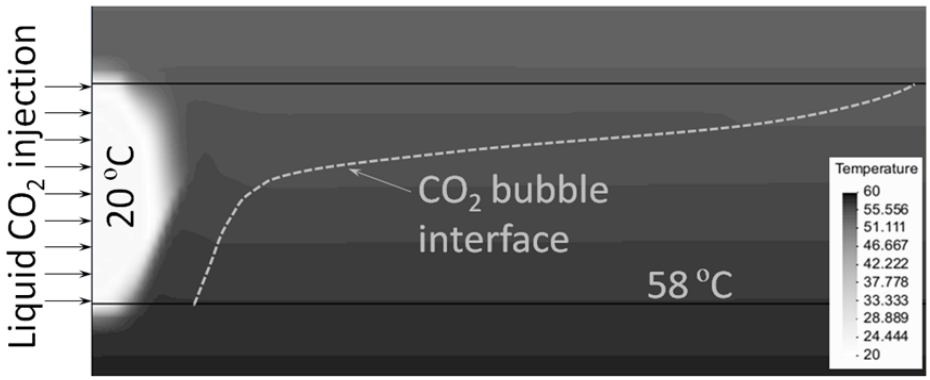

Figure 3.14: Temperature after 8 months of liquid CO_2 injection

Pressure effects on CO_2 plume evolution

Injection pressures for liquid CO_2 will be slightly lower than for SC CO_2 (Figure 3.15 (a)) because a higher CO_2 density reduces the volumetric flow rate and therefore the pressure build up around the well. Furthermore, the overpressure in the whole aquifer is reduced when injecting liquid CO_2 (Figure 3.15 (b)), which improves the mechanical stability of the caprock (Vilarrasa et al, 2013).

On other hand, Figure 3.16 displays the overpressure normalized by the effective lithostatic stress that is needed to induce a microseismic event at the top of an aquifer at 1500 m depth when injecting cold CO_2. It is a function of the friction angle for several temperature changes, for a lateral earth pressure coefficient of 0.5 and a Poisson's ratio of 0.3. Obviously, the aquifer can support higher overpressures as its friction angle increases. But micro-seismicity is induced within the reservoir by lower overpressures when the temperature contrast increases. Furthermore, the stiffer the rock, the lower the overpressure needed to reach the failure envelope within the aquifer for a given temperature change.

(a)

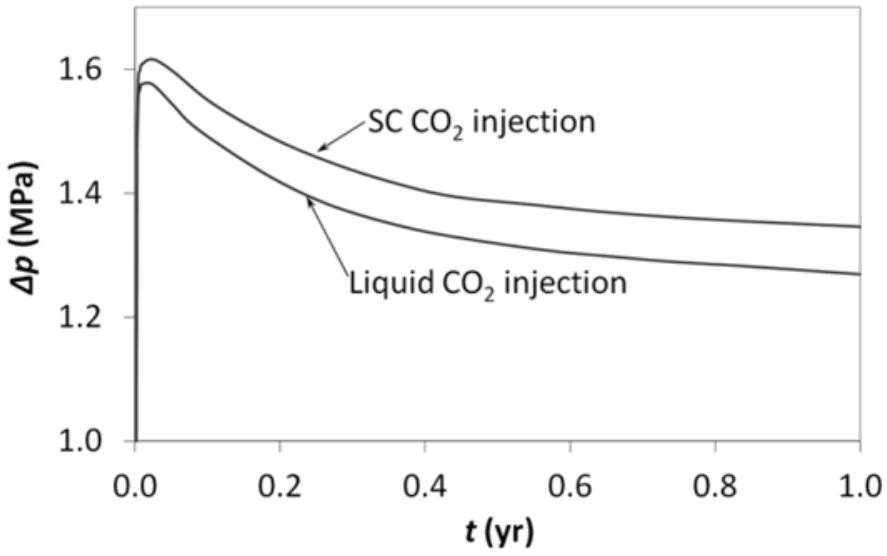

(b)

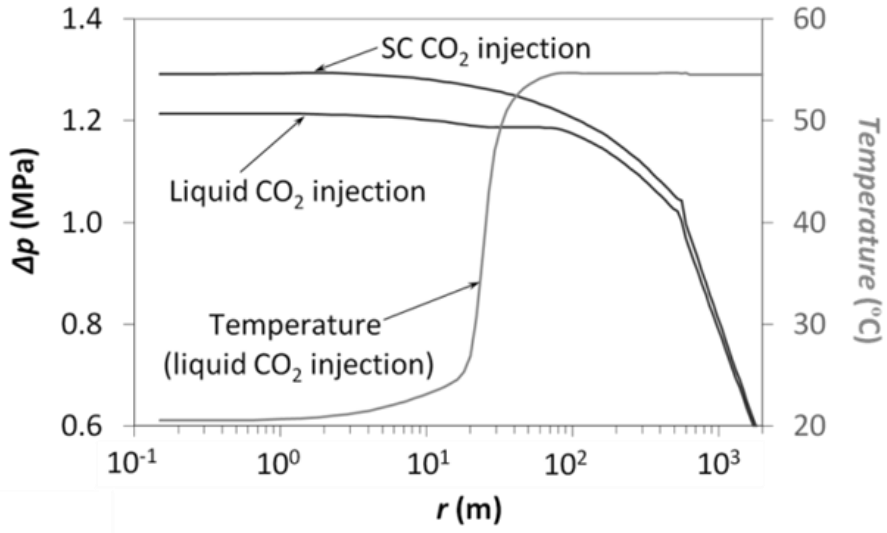

Figure 3.15: (a) Overpressure evolution at the top of the storage formation in the injection well for liquid and SC CO_2 injection and (b) fluid pressure at the top of the aquifer as a function of radial distance from the injection well after 1 yr of injection.

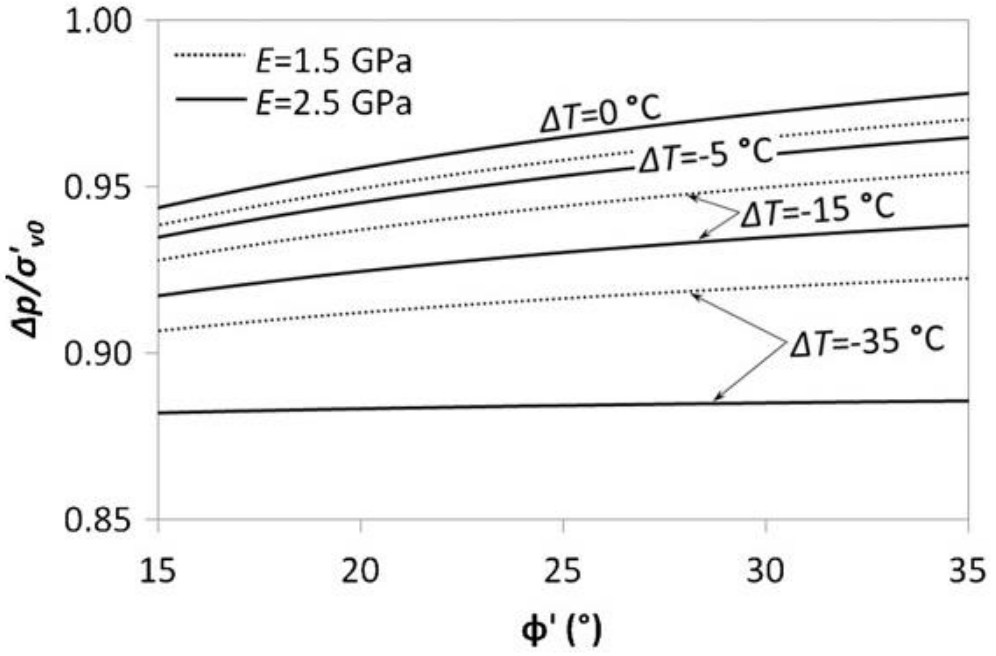

Figure 3.16: Overpressure normalized by the effective lithostatic stress that is needed to induce a microseismic event at the top of a storage formation placed at 1500 m depth when injecting CO_2 at several temperatures as a function of the friction angle for a lateral earth pressure coefficient of 0.5 and a Poisson ratio of 0.3

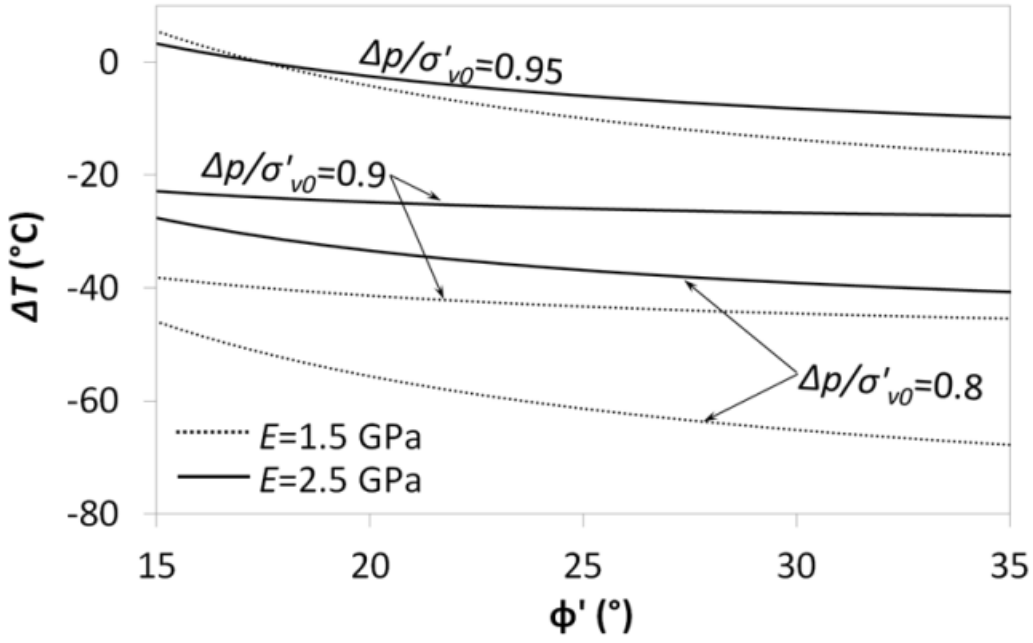

Figure 3.17: Temperature drop that is needed to induce a microseismic event at the top of a storage formation placed at 1500 m depth when injecting CO_2 at several overpressures (normalized by the effective lithostatic stress), respectively, as a function of the friction angle for a lateral earth pressure coefficient of 0.5 and a Poisson ratio of 0.3

Figure 3.17 displays the temperature change that is needed to induce a microseismic event at the top of a storage formation placed at 1500 m depth when injecting cold CO_2, as a function of the friction angle for several overpressures for a lateral earth pressure coefficient of 0.5 and a Poisson ratio of 0.3. The maximum acceptable temperature change for a given overpressure increases with the friction angle. Furthermore, the stiffer the rock, the smaller the temperature change required for inducing micro-seismicity within the reservoir for a given overpressure. The use of Figure 3.17 is recommended as a preliminary analysis of the suitability of liquid CO_2 injection at a given site, to avoid the high computational cost of coupled thermo-hydro-mechanical simulations (Vilarrasa et al, 2013).

3.3.3. Operational conditions and test procedure

Liquid CO_2 injection requires careful thermodynamic modelling of all processes that take place during the transition that occurs when starting the injection.

As shown in Figure 3.2, the sudden expansion of cold CO_2 produces a sudden cooling. The problem can be described in terms of energy. The energy (enthalpy) of the gas is much higher than that of the liquid, which in turn is greater than that of the solid. In parallel, the energy of the molecules increases with pressure as function of compressibility. The sudden expansion takes place with little heat exchange outside the plume.

This indicates that in the early stages of injection, solidification could occur only in spaces initially filled with CO_2, although this is not the situation at Hontomin. It is evident that the sudden expansion of the CO_2 must be avoided; this could happen when the casing is connected to a pipe with higher pressure (filled with liquid CO_2 at high pressure, not less than 20 bar). To avoid this, it would be possible to inject CO_2 or an inert gas (e.g. N_2) in the wellhead until it reaches a pressure equal to the operation before turning the pump on or connecting the wellhead to the outlet pipe of the pump.

The procedure would be:

1) Inject CO_2 or an inert gas at the wellhead. In the case of CO_2, this operation should connect the wellhead with the CO_2 storage tank. At the beginning, the operation should be slow enough to ensure thermal equilibrium with the environment. That is to say, CO_2 would be in gas phase.

2) Without disconnecting the head, activate the CO_2 pump. The pressure would balance with the CO_{22} in the well. As pressure increases and water flows, the initial CO_2 will liquefy.

CO_2 is likely to be in a gaseous state at the top of the well tubing, especially in the absence of pumping, where CO_2 could be extracted directly from the top of the tank to prevent boiling in the pipes.

3.3.4. Comparison with SC CO_2 injection

CO_2 behaviour in the injection well

We summarize the results of Vilarrasa et al, (2013b), which include several operational conditions at the wellhead to compare the feasibility and energy consumption of the proposed injection with other schemes.

Table 3.3 displays the pressure and temperature values for five injection conditions at the wellhead: gas-phase, near-critical point, supercritical phase, liquid-phase at high pressure and temperature and liquid-phase at low pressure and temperature. Supercritical injection requires higher pressure and energy consumption.

Table 3.3: Several CO_2 injection conditions at the wellhead and their estimated compression energy consumption.

Injection conditions at the wellhead	*T*, ºC	*p*, MPa	Energy consumption, kW
Gas-phase	35	6.5	409.6
Near-critical point	31	7.0	368.2
Supercritical phase	40	8.0	361.9
Liquid-phase (high *T* and *p*)	25	8.0	154.7
Liquid-phase (low *T* and *p*)	5	4.2	83.6

Figure 3.18 shows that injection in gas and supercritical phase conditions causes a distribution of low densities along the wellbore.

Injecting gaseous CO_2 in near-critical point conditions causes a two-phase flow pattern within the injection pipe near the surface (in the first 50 m). It should be noted that phase changes lead to higher head losses in pipes and are generally avoided for CO_2 transport, but are of little concern here because head losses are very small. This two-phase flow behaviour is associated with a change in the slope of the temperature profile when the fluid becomes supercritical. The resulting change of phase leads to higher densities through the injection pipe than those obtained when injecting in gas and supercritical phase conditions.

In contrast, the injection of CO_2 in liquid-phase conditions leads to a high CO_2 density, which is comparable to that of brine, along the entire injection pipe. CO_2 temperature stays nearly constant through a long section of the pipe and then increases slightly due to heat exchange with the surroundings. When injecting at high pressure and temperature, the fluid undergoes slight cooling in the upper portion because of the heat exchange with the encasing rock. Subsequently, CO_2 pressure at the bottom of the well becomes very high, around 20 MPa for these particular injection conditions, because the injection at the wellhead is made at high pressure. To alleviate this issue, overpressure can be avoided at the bottom of the well by injecting liquid CO_2 at low pressure and temperature, resulting in a CO_2 pressure similar to that obtained when injecting in near-critical conditions, i.e. around 17 MPa (Vilarrasa et al, 2013b).

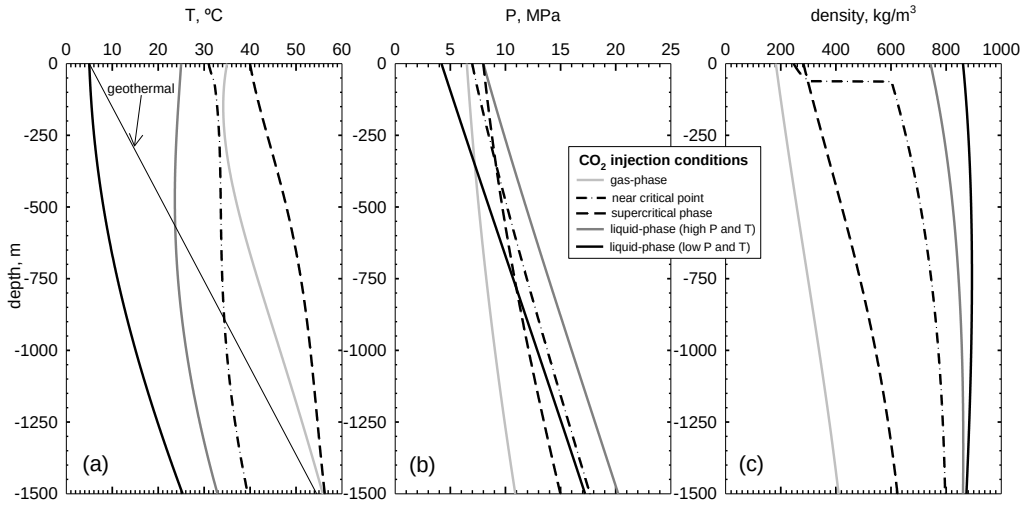

Figure 3.18: Flow of CO_2 through an injection well: temperature (a), pressure (b) and density (c) profiles. Comparison between different injection conditions at the wellhead (gas-, supercritical- and liquid-phase). (Vilarrasa et al, 2013a).

Mechanical stability

Pressure and temperature changes induce strain and stress changes. Figure 3.19 displays the horizontal and vertical displacements of SC and liquid CO_2 injection. Since fluid pressure distribution is quite similar in both injections Figure 3.15), the differences in displacements will be due to thermal effects. SC CO_2 injection (isothermal) produces a vertical expansion of the storage formation, pushing upwards on the caprock and slightly downwards on the seal below the aquifer. Laterally, SC CO_2 injection pushes the formation water/brine away from the injection well. However, liquid CO_2 injection generates a cold region around the injection well that undergoes thermal contraction. This is reflected in both the vertical and horizontal displacements. Vertically, the caprock moves downwards and the seal below the aquifer moves upwards close to the injection well. Similarly, the aquifer is displaced toward the injection well in the cold region, presenting the maximum negative horizontal displacement at the cold temperature front. Further away, the aquifer expands both vertically and horizontally due to overpressure (Vilarrasa et al, 2013).

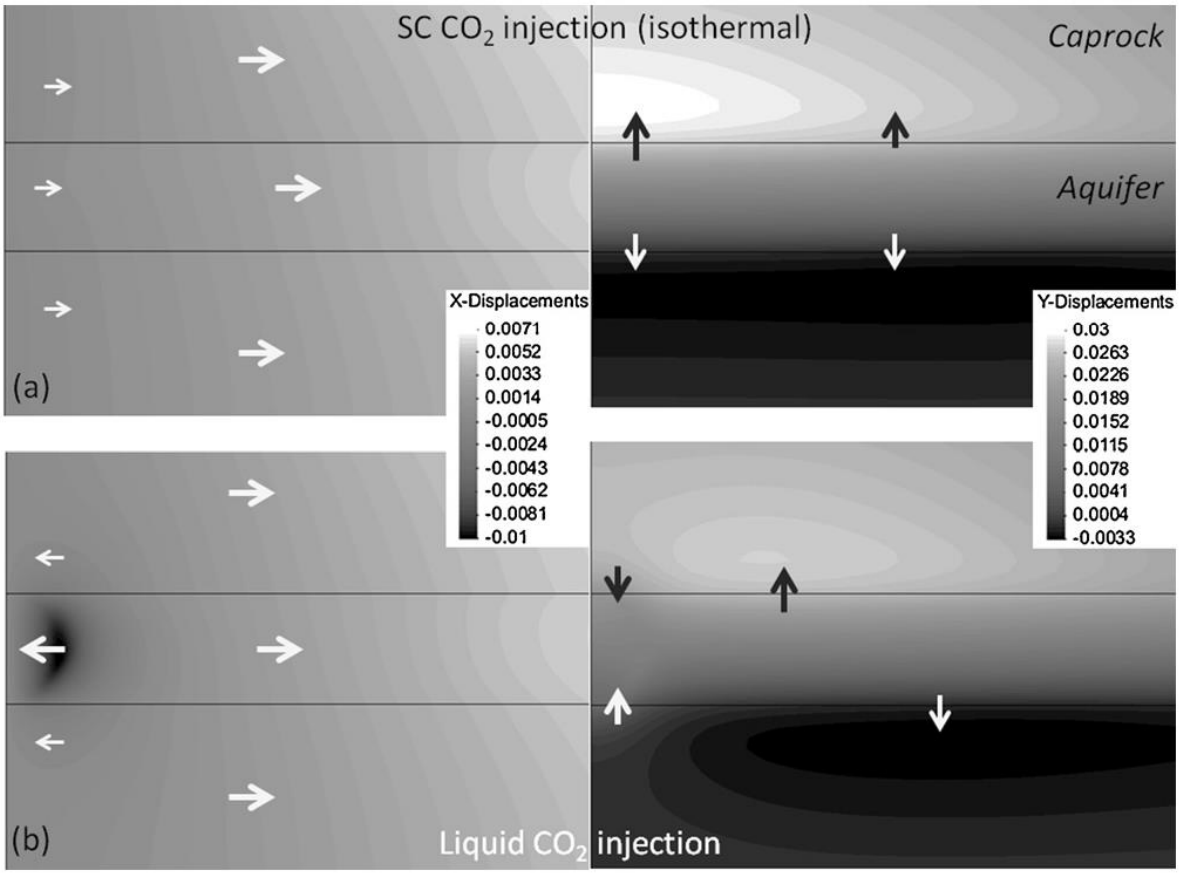

Figure 3.19: Horizontal and vertical displacements of (a) supercritical and (b) liquid CO_2 injection. Fluid injection pushes the formation laterally and expands it vertically. When injecting cold CO_2, the thermal contraction of the rock is superimposed to the hydraulic effect. The arrows indicate the direction of the displacement. The injection point is located midway on the left hand side.

Figure 3.20 displays total stress changes as a function of depth 3 m away from the injection well after 8 months of injecting liquid and SC CO_2. The stress change is almost symmetric with respect to the middle of the aquifer. The vertical stress remains practically unaltered when injecting SC CO_2. However, it is reduced as a result of temperature drop when injecting liquid CO_2, with the maximum stress reduction in the middle of the aquifer. The stress reduction is also significant in the region of the seals affected by the temperature reduction (recall Figure 3.14). The horizontal stresses increase in the aquifer because of lateral confinement that opposes the expansion caused by CO_2 injection. The stress reduction due to thermal contraction of the rock superimposes this horizontal stress increment, resulting in an overall stress reduction in the aquifer when injecting liquid CO_2. The stress reduction due to thermal contraction of the rock is similar in magnitude in the vertical and horizontal directions. The fact that vertical stresses decrease in the aquifer produces an increase of the horizontal stresses in the seals close to their contact with the aquifer. This can be explained by an arch effect that is formed around the volume with vertical stress reduction able to support overburden on top of the aquifer.

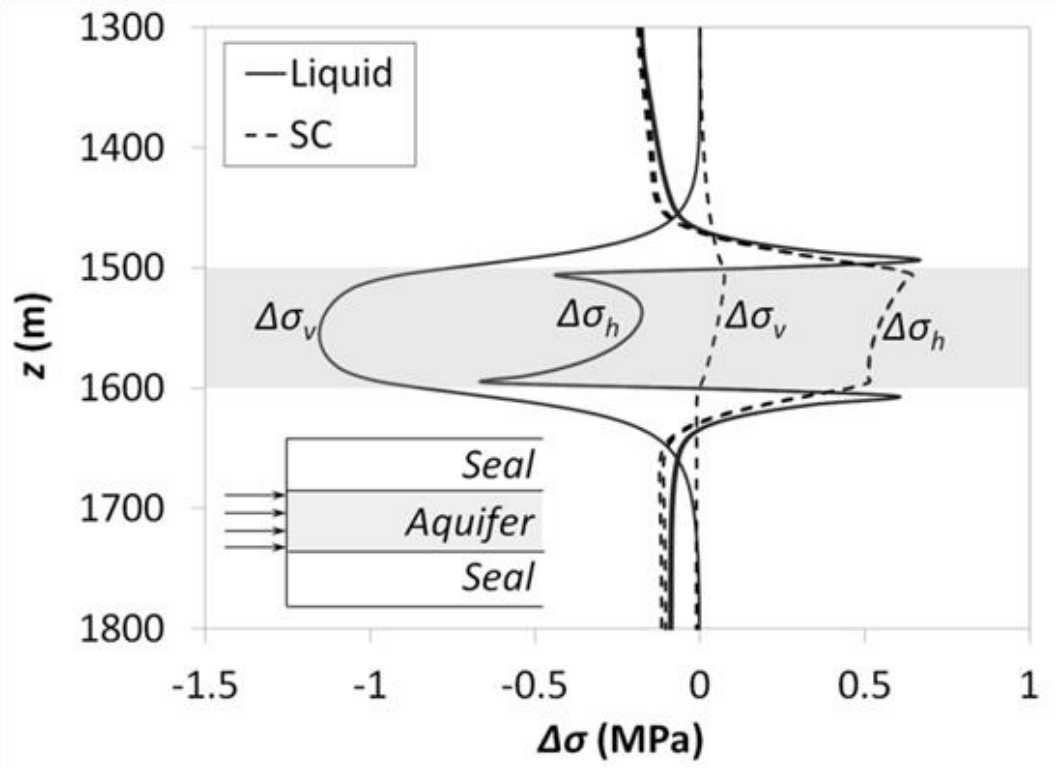

Figure 3.20: Changes in total stress as a function of depth 3m away from the injection well for liquid and SC CO_2 injection after 8 months of injection.

Fluid injection induces an effective stress reduction that brings the stress state closer to the failure envelope. Furthermore, if the fluid is colder than the formation, a thermal contraction of the rock will occur, further reducing the effective stresses. However, liquid CO_2 injection benefits from a lower overpressure for a given mass flow rate.

To conclude, thermal effects on mechanical stability can be pronounced for large temperature contrasts and stiff rocks (e.g. Hontomin). Thermal contraction mobilizes higher friction angles in the aquifer, which could lead to shear slip of pre-existing fractures. The effect of shear slip can be advantageous within the aquifer, enhancing permeability and thus CO_2 injectivity. Interestingly, the mobilized friction angle in the seals is not increased when injecting liquid CO_2 and it is even reduced in stress regimes where the maximum principal stress is vertical (Vilarrasa et al, 2013).

3.4. INTERMITTENT INJECTION

CO_2 may be injected continuously with a more or less constant rate or intermittently, i.e. alternated with periods of no injection. Intermittent injection causes more heterogeneity of flow and hence dispersion, which in its turn causes more CO_2 to mix with and dissolve into saline water. Therefore, intermittent injection may have an advantage over continuous injection.

To evaluate the effect of intermittent injection we first studied how the CO_2 plume evolves after an injection is stopped. For this purpose, a continuous injection of $2.5.10^9$ kg CO_2 $year^{-1}$ in a 100 m thick calcareous aquifer of 10 and 100 mD was simulated. These two values of permeability have been chosen to illustrate how changes in permeability could affect intermittent injection. We changed this model by stopping injection after 100 days. The goal was to analyse saturation changes and find the minimum time required to produce significant movement in the CO_2 plume. To this end, we used the

approach of Saaltink et al. (2013), who solved the coupled multiphase flow and reactive transport problem using a simplified approach for the case in which reactions can be assumed to occur close to equilibrium. This is a reasonable assumption for calcite and most carbonate minerals, because the dissolution kinetics are usually very rapid with high pressure CO_2 gas near the critical point.

We used a simple axisymmetric geometry of a 100 m thick homogeneous horizontal formation at 1500 m depth. The model extends 5 km laterally. An injection well with a radius of 0.15 m is placed in the centre of the domain (fig. 3-21) where the liquid CO_2 injection is injected along the entire borehole.

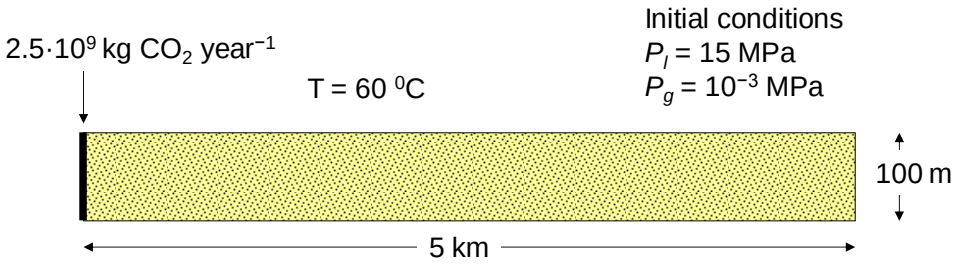

Figure 3.21: Schematic description of the conceptual model used in all simulations.

Figure 3. shows the saturation after 100 days of injecting at a flow rate of 0.84 $kg \cdot s^{-1}$. Also shown are the saturations after 1 year of rest. Figure 3., shows the increase or decrease of saturation after stopping injection; CO_2 flows upwards and spreads laterally at the upper part of the aquifer. Thus the CO_2 phase near the injection well in the lower part of the aquifer is replaced by brine. Interestingly, the CO_2 pressure in this part of the aquifer remains high (Figure 3.) despite the brine flowing towards the well from zones with relative low CO_2 pressure. Vertical mixing is high enough to transport CO_2 from the plume downwards. This also keeps the density of the liquid in this zone high (Figure 3. and Figure 3.).

Porosity or calcite dissolution is not affected significantly by the retreat of the CO_2 plume at the lower part of the aquifer (Figure 3.). Only at the top of the aquifer, where the CO_2 plume still advances, does the porosity increase due to calcite dissolution. In fact, it is interesting to observe (i) that dissolution is most clearly marked when the CO_2 invasion occurs at rest than under injection and (ii) that some precipitation occurs in the lowest portion of the storage formation (more noticeable for the 10mD case than for the 100mD case). This calcite precipitation reflected the significant reduction in CO_2 pressure. The velocity of the brine decreases after injection is stopped with the exception of the upward velocity near the well for the case of the highest permeability of 100 mD (Figure 3.).

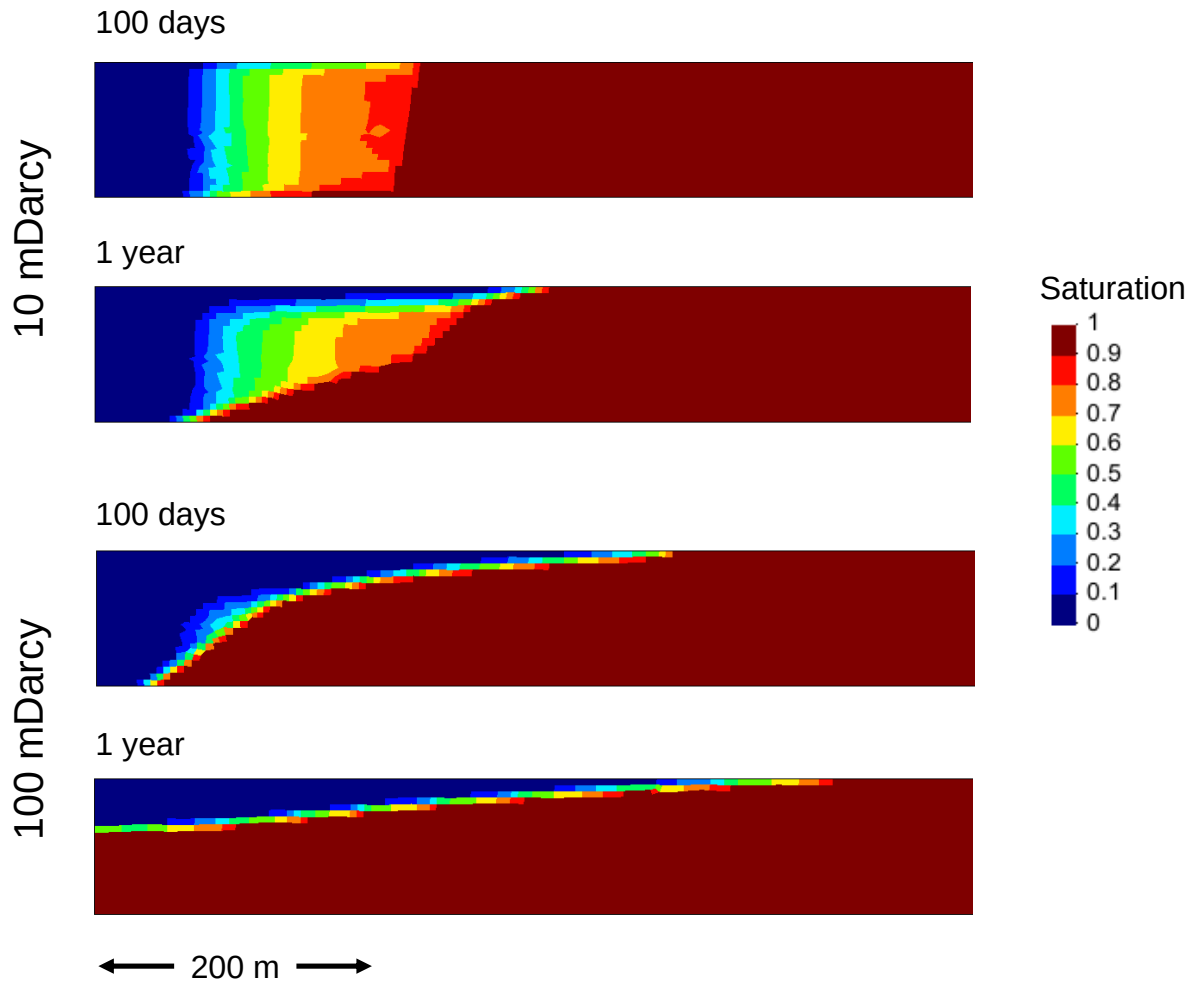

Figure 3.21: Saturations in aquifers of 10mD (top) and 100mD (bottom) after injection CO_2 during 100 days, stopping injection and letting the CO_2 plume rest until t=1year. Injection well is located on the left side of the images.

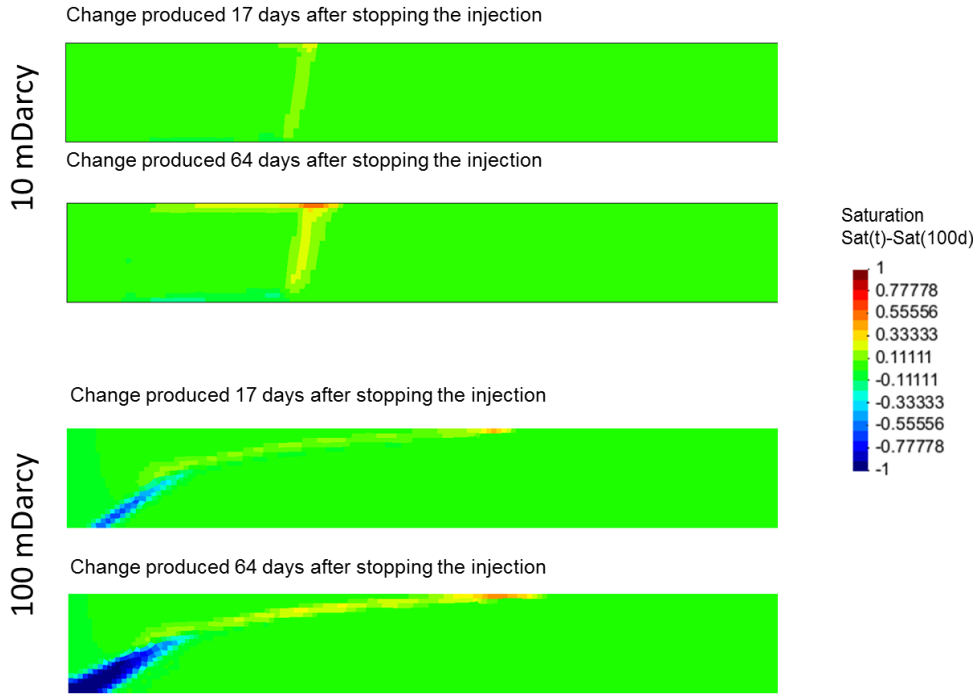

Figure 3.22: Changes in saturation produced after 17 and 64 days after stopping CO_2 injection, which lasted 100 days. Injection well is located on the left side of the images.

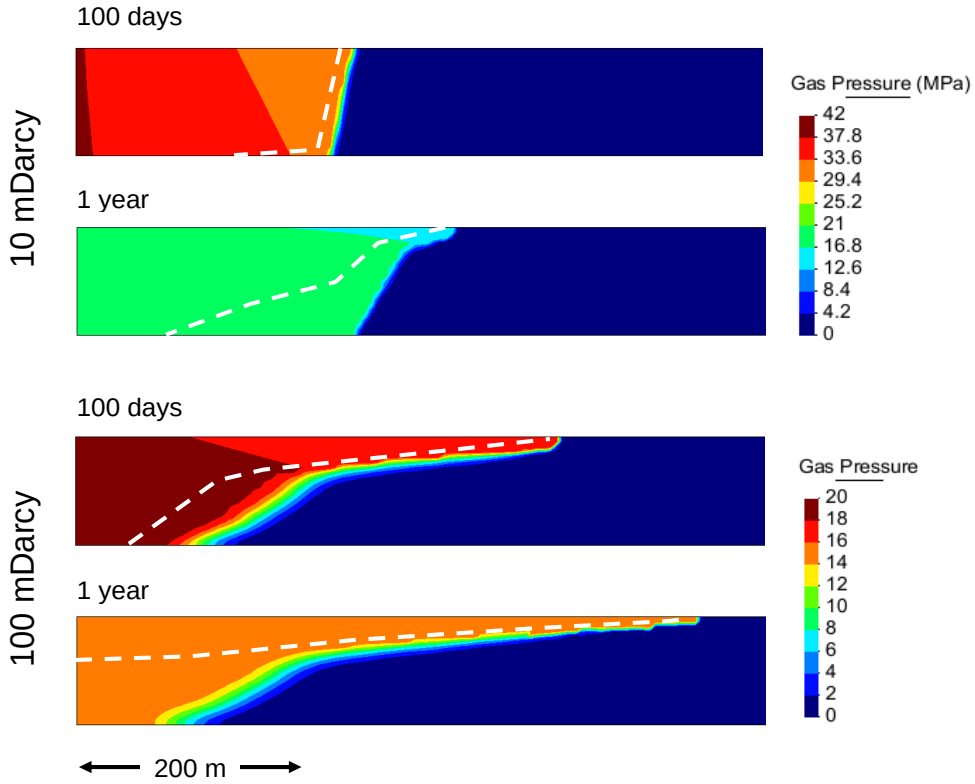

Figure 3.23: CO_2 pressure partial pressure of dissolved CO_2 when less than 16 bar) after 100 days. The dashed line indicates the CO_2 plume (saturation = 0.9). Injection well is located on the left side of the images.

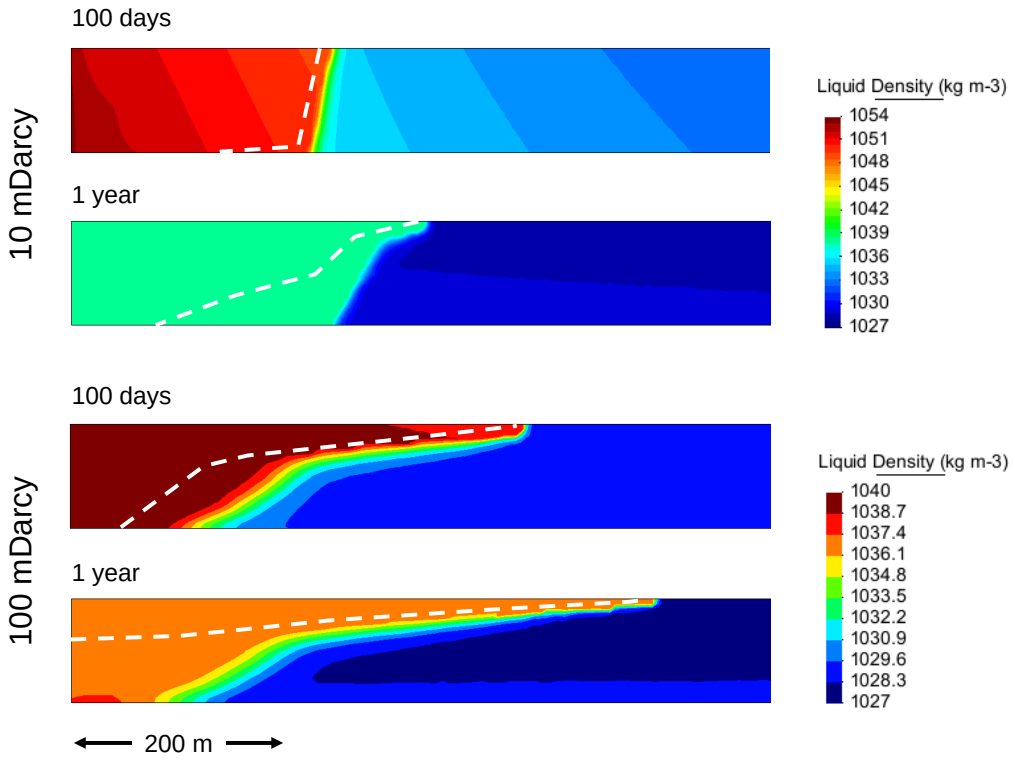

Figure 3.24: Density of the brine after 100 days of injection and after 265 days of rest. The dashed line indicates the CO_2 plume (saturation = 0.9). Injection well is located on the left side of the images.

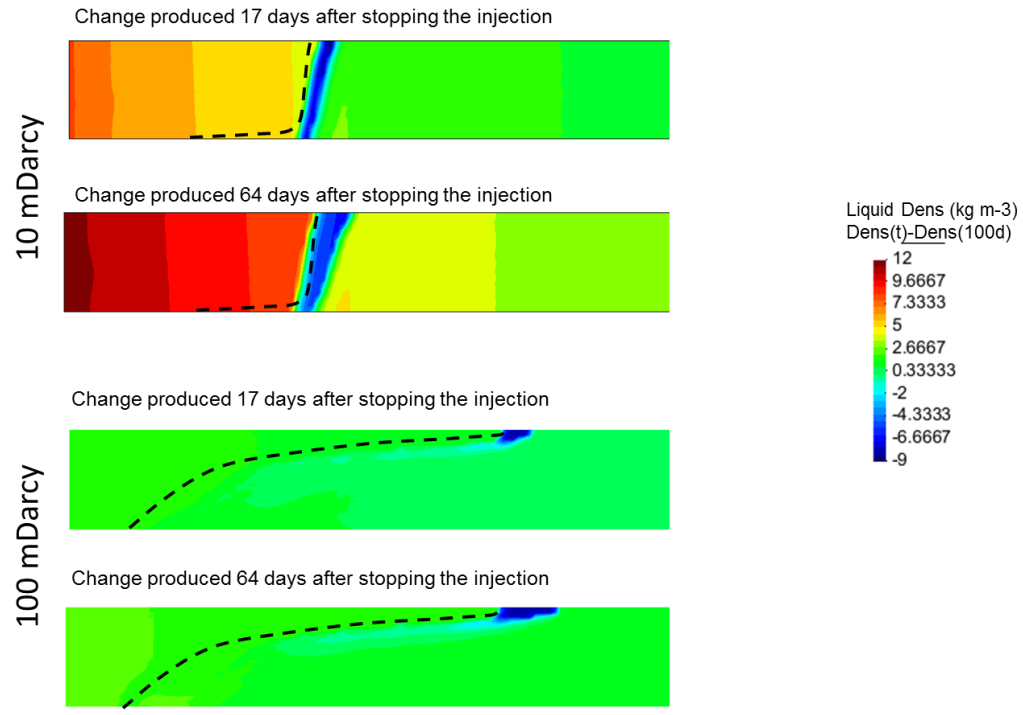

Figure 3.25: Liquid density change produced 17 and 64 days after the liquid CO_2 injection stops. The dashed line indicates the CO_2 plume (saturation = 0.9). Injection well is located on the left side of the images.

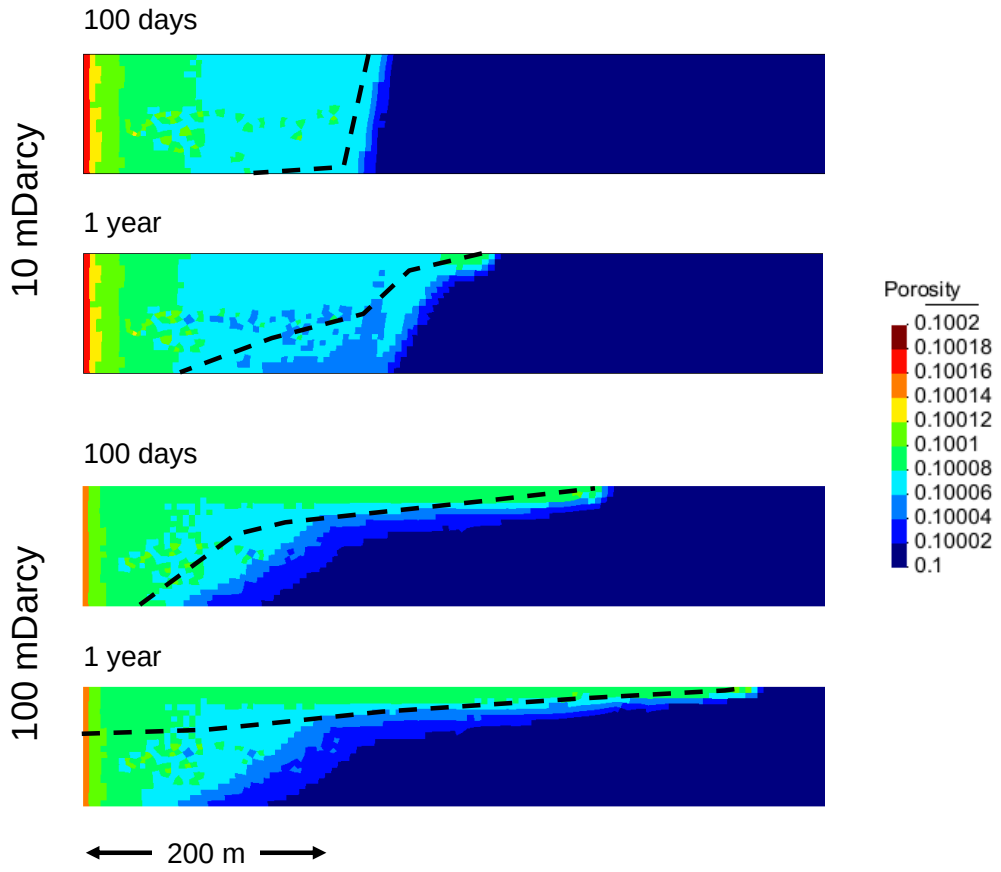

Figure 3.26: Porosity after 100 days (when CO_2 injection stops) and 1 year for both models. The dashed line indicates the CO_2 plume (saturation = 0.9). Injection well is located on the left side of the images.

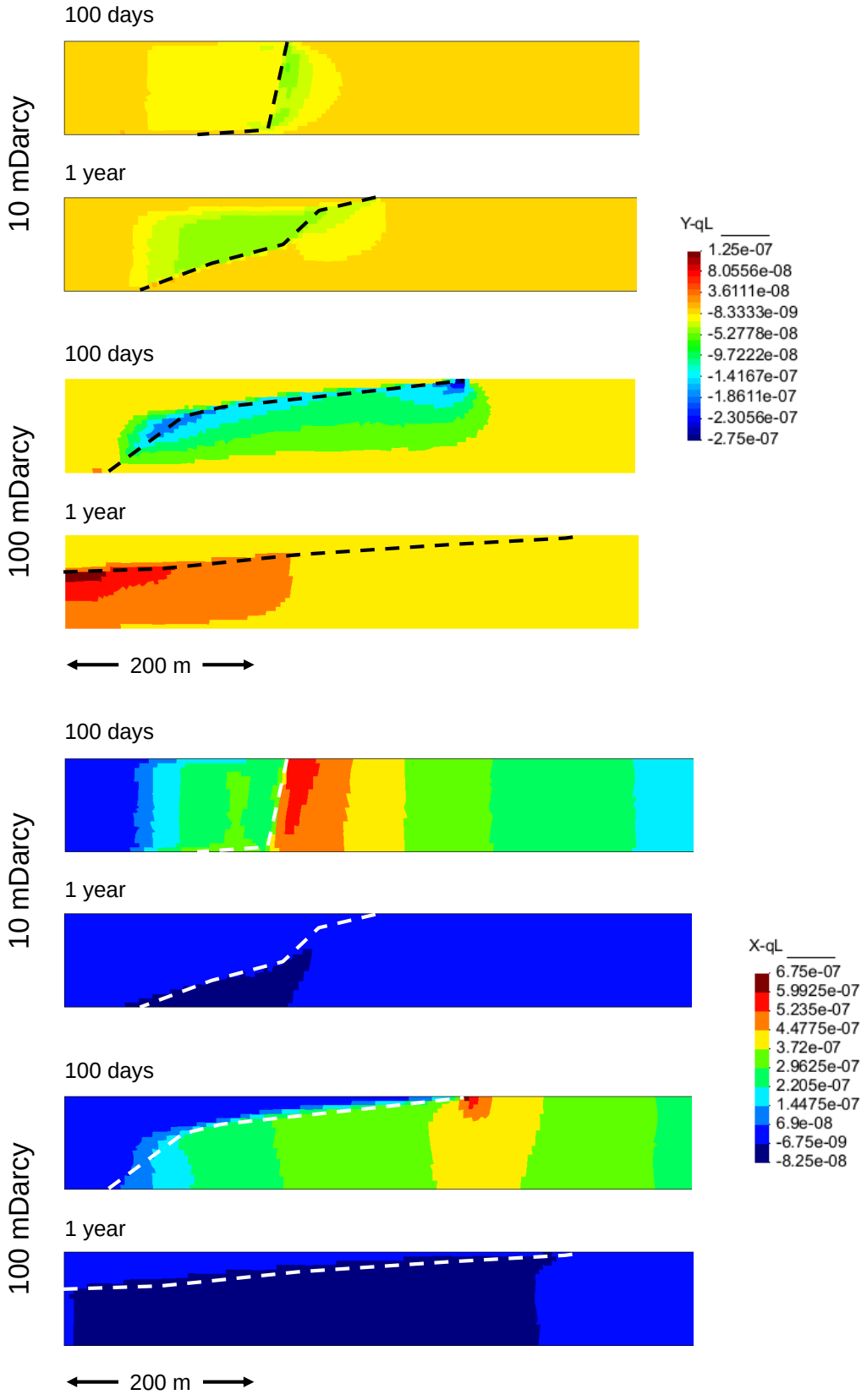

Figure 3.27: Vertical (top four figures) and horizontal (bottom four figures) Darcy flux of brine after 100 days (when CO_2 injection stops) and 1 year for both models. The dashed line indicates the CO_2 plume (saturation = 0.9). Injection well is located on the left side of the images.

3.5. INTERACTION BETWEEN TESTS

This section contains a brief discussion of a proposed sequence of tests to meet project objectives. The basic assumptions of the proposal are as follows:

1) The push-pull test should be performed prior to any other test, both to avoid interferences caused by the high compressibility of the CO_2 plume and because large amounts of CO_2 would have to be vented in order to ensure residual CO_2 conditions, if a large amount of CO_2 had been injected prior to pull.

2) The liquid injection test causes a cooling of the storage formation that would have to be warmed up to recover natural conditions. Therefore, SC injection tests must be performed prior to cold injection.

3) Intermittent injection does not significantly affect either cold or SC injection tests. In fact, injection shut downs will occur in many operations because of maintenance operations. These can be considered opportunities for monitoring various parameters in response to fluctuations in injection rate.

In view of the above, the proposed test sequence is as follows:

(1) Push-pull test, following the procedure explained in section 3.1.3. An injection volume of 200 tons has been suggested, but the amount is not fixed.

(2) Supercritical injection test, following the procedure explained in section 3.2.3. We have not stated any minimum amount of CO_2 injection.

(3) Cold CO_2 injection, following the procedure stated in section 3.3.3.

(4) Periodic stops in injection rate should occur either during SC or liquid injection or both. Since repeatability is not possible, the increase in CO_2 dissolution can only be assessed by means of modelling.

4. DISCUSSION and CONCLUSIONS

Hontomín, CIUDEN's site for testing CO_2 storage, displays two important features. Firstly, reservoir permeability and porosity are very low. Secondly, the storage formation is composed of carbonate rocks. This report addresses the second feature.

Injection of CO_2 in carbonate rocks has been studied because the resident water (brine) will be acidified by CO_2 dissolution. Acidity promotes dissolution of carbonates. This concept is swell established and has raised concerns that injecting CO_2 into carbonate rocks could lead to the formation of cavities, which in turn might compromise the stability of the storage formation and caprock.

Large-scale simulations of CO_2 injection into carbonate formations have been simulated to understand the overall amount of carbonate that can be dissolved. Small-scale laboratory experiments were undertaken to understand the conditions under which dissolution might become localized, forming wormholes.

An improved model has been used to simulate multiphase flow and reactive transport. The model includes the displacement of brine by supercritical CO_2 (1500 m depth, 60ºC), the dissolution of CO_2 in the brine, its acidification, and the resulting dissolution of carbonate. Two cases have been considered for permeability: 100 mD, which soon leads to density dominated flow (i.e., the CO_2 tends to float on top of the brine) and 10 mD, which maintains viscous dominated flow conditions (i.e., cylindrical push away from the injection well) for much longer. In both cases, overall dissolution is small (porosity increases of less than 2.10^{-4}) and restricted to the outer edge of the CO_2 plume. The conclusion is that formation of large cavities is highly unlikely.

Insight into the conditions for wormhole formation was gained through laboratory experiments. Results from these experiments showed that calcite dissolution may become localized, depending on the flux of undersaturated brine and dissolution kinetics. In the two extreme cases (infinitely fast transport or kinetics), dissolution is homogeneous. However for a broad range of conditions, dissolution tends to form wormholes. While this may appear to contradict the large-scale numerical model, it should be noted that wormhole formation is a small-scale heterogeneous process. Secondly, even if localized dissolution conditions are met, thousands of pore volumes need to flow through the medium for wormholes to become significant. This condition will not occur under normal CO_2 storage conditions, but dissolution localization might occur under intermittent CO_2 injection, which should be assessed in further projects.

Injection strategies proposed for Hontomin have been assessed for wider use, with many of the findings not specific to carbonate rocks. The sequence of injection tests proposed for Hontomín includes: (1) Push-pull CO_2 injection tests, proposed specifically to improve site characterization, especially with regards to capillary trapping; (2) Supercritical injection, which is proposed as a reference benchmark; (3) Liquid phase (i.e., cold and dense) CO_2 injection, which is proposed as a way to reduce compression costs at the wellhead; and (4) Pulsed (intermittent) injection, which is proposed as way to accelerate dissolution of CO_2 into the resident brine. For each of these tests, the expected plume shape and size were analyzed and operational conditions described. We conclude that the strategy least costly and least demanding from an operational viewpoint is the injection in liquid phase – provide risks of fracturing can be managed. However, any of the above strategies may be appropriate for CO_2 geological storage, subject to site specific conditions.

5. ACKNOWLEDGEMENTS

This work has been carried out in the context of the contract with reference number FPA041, between the Global CCS Institute and Fundación Ciudad de la Energía (CIUDEN), with the collaboration of GHS-CSIC-UPC research group. Some of the developments have been funded by the European Commission through the MUSTANG and the PANACEA projects (Seventh Framework Programme FP7/2007-2013 under grant agreements nº 227286 and nº 282900, respectively).

6. REFERENCES

Ahmad, M., Gernert, J., Wilbers M., (2014). Effect of impurities in captured CO_2 on liquid–vapor equilibrium. Fluid Phase Equilibria Vol 363, Pages 149–155.

Akgerman, A. and Giridhar, M., (1994). "Fundamentals of Solids Extraction by Supercritical Fluids," In Supercritical Fluids - Fundamentals for Applications; Sengers, J.M.H.; Kiran, E., Eds., Klüwer Academic Publishers, pp:669-696.

Al-Siyabi, I. Effect of impurities on CO_2 stream properties. Heriot-Watt University Institute of Petroleum Engineering. February 2013.

Archie, G. E. (1952). Classification of carbonate reservoir rocks and petrophysical considerations. AAPG Bull. 36: 278

Bachu, S., Gunter, W.D., Perkins, E.H., (1994). Aquifer disposal of CO_2 - hydrodynamic and mineral trapping. Energy Conversion and Management 35, 269-279.

Bagrintseva, K. I. (1977). Carbonate Rocks, Oil and Gas Reservoirs. Izdated ' stvo Nedra , Moscow , 231pp

Bao, J., Hou, Z., Fang, Y., Ren, H., Lin, G., (2013a): Uncertainty quantification for evaluating impacts of caprock and reservoir properties on pressure buildup and ground-surface displacement during geological CO_2 sequestration. Greenhouse Gases: Science and Technology, http://dx.doi.org/10.1002/ghg.1362.

Bao, J., Xu, Z., Lin, G., Fang, Y., (2013b) Evaluating the impact of aquifer layer properties on geo-mechanical response during CO_2 geological sequestration. Computers &Geosciences 54, 28–37.

Berg, R. R. (1970). Method for determining permeability from reservoir rock properties. Gulf Coast Assoc. Geol. Soc. Trans.20: 303 – 3

Bieniawski, Z. T., (1978). "Determining rock mass deformability: experience from case histories." *International Journal of Rock Mechanics and Mining Sciences & Geomechanics Abstracts*. Vol. 15. No. 5. Pergamon.

Blunt M.J., Bijeljic B., Dong H., Gharbi O., Iglauer S., Mostaghimi, P.A. Paluszny, C. (2012). Pentland Pore-scale imaging and modelling, Advances in Water Resources, 51, pp. 197–216Bachu, S. (2003): Screening and ranking of sedimentary basins for sequestration of CO_2 in geological media in response to climate change. Environ. Geol. 44, 277–289

Coquelet C., Valtz A., Dieu F., Richon D., Arpentinier P., Lockwood, P., (2008). Isothermal *x*,*y* data for the argon + carbon dioxide system at six temperatures from 233.32 to 299.21 K and pressures up to 14 MPa. Fluid Phase Equilibria, 273 (1), pp. 38–43

Chadwick et al. 2007. Pag.31. Best Practice for the storage of CO_2 in saline aquifers. Observations & Guidelines from the SACS & CO_2STORE Projects.

ChemicaLogic Corporation (1999) Thermodynamic and transport properties of carbon dioxide, , 8 Cedar Street, Suite 56, Woburn MA, 01801 USA. www.chemicalogic.com

Choquette, P.W. and L.C. Pray, (1970). Geologic nomenclature and classification of porosity in sedimentary carbonates: AAPG Bulletin, v. 54/2, p. 207-244.

Cortés V.J., B.Navarrete y M.Lupión (2013): Captura, transporte y almacenamiento del CO_2 originado por el empleo de combustibles fósiles. Fundación Ciudad de la Energía (CIUDEN)

Craze, R. C., (1950). Performance of limestone reservoirs. Trans. AIME 189 : 287 –294

Cubillo, B., Martinez-Landa, L., Carrera, J., Rötting, T.S., Silva, O., (2012). Application of Thermal response test to distributed fiber-optic temperature sensor (DTS) for CO_2 storage at Hontomín Technological Development Plant, EGU General Assembly 2012, Vienna, pp. EGU2012-9605.

de Simone, S., Vilarrasa, V., Carrera, J., Alcolea, A., Meier, P., (2013): Thermal coupling may control mechanical stability of geothermal reservoirs during cold water injection. Journal of Physics and Chemistry of the Earth 64, 117–126.

Dentz, M., Tartakovsky, D.M. (2009): Abrupt-interface solution for carbon dioxide injection into porous media. Transp. Porous Media 79, 15–27

E-on Report (2011), Project, E. U., Equation of state prediction of carbon dioxide properties. Kingsnorth carbon capture & storage project, Tech. rep., CP-GNS-FAS-DRP-0001. http://www. decc.gov.uk/assets/decc/11/ccs/chapter6/6.23-equation-of-state-prediction-of-carbon-dioxide-properties.pdf,

Eriksson, M. (2009) Impurities in Carbon Dioxide Capture and Transport. PhD Thesis, NTNU, department of petroleum engineering and applied geophysics. Trondheim, July 2009.

Ferronato,M., Gambolati, G., Janna, C., Teatini, P. (2010): Geomechanical issues of anthropogenic CO_2 sequestration in exploited gas fields. Energy Convers. Manage. 51, 1918–1928

Flügel, E. (2004). Microfacies of Carbonate Rocks Springer-Verlag, Berlin, p. 976.

Freifeld, B.M., Finsterle, S., Onstott, T.C., Toole, P., Pratt, L.M., (2008). Ground surface temperature reconstructions: Using in situ estimates for thermal conductivity acquired with a fiber-optic distributed thermal perturbation sensor. Geophysical Research Letters 35.

Freifeld, B.M., Daley, T.M., Hovorka, S.D., Henninges, J., Underschultz, J., Sharma, S., (2009). Recent advances in well-based monitoring of CO(2) sequestration, in: Gale, J.H.H.B.J. (Ed.), Greenhouse Gas Control Technologies 9, pp. 2277-2284.

GCCSI (2010): Good plant design and operation for onshore carbon capture installations and onshore pipelines, a recommended practice guidance document. First edition. Energy Institute (CCSa, GCCSI), London. September 2010.

Ghassemi, A., Tarasovs, S., Cheng, A.H.-D., (2007): A 3-D study of the effects of thermomechanical loads on fracture slip in enhanced geothermal reservoirs. International Journal of Rock Mechanics and Mining Sciences 44, 1132–1148.

Gomes, J.S., M.T. Ribeiro, C.J. Strohmenger, S. Negahban, M.Z. Kalam, (2008). Carbonate reservoir rock typing – the link between geology and SCAL, Abu Dhabi International Petroleum Exhibition and Conference, 3-6 November 2008, SPE, Abu Dhabi, UAE, p. 14

Goos E., Riedel U., Zhao L., Blum L. , (2011). Phase diagrams of CO_2 and CO_2–N_2 gas mixtures and their application in compression processes, Energy Procedia 4, pp:3778–3785 (10th International Conference on Greenhouse Gas Control Technologies).

Hailong Li. Thermodynamic Properties of CO_2 Mixtures and Their Applications in Advanced Power Cycles with CO_2 Capture Processes, PhD Thesis, Royal Institute of Technology, Stockholm (Sweden), September 2008.

Hamon, G., (2003). Two-phase flow rock-typing: another perspective, SPE Annual Technical Conference and Exhibition, 5–8 October 2003: Denver, Colorado, p. 12

Heuze, Francois E., (1980). "Scale effects in the determination of rock mass strength and deformability." Rock Mechanics 12.3-4.

Hidalgo, J.J., Carrera, J, 2009. Effect of dispersion on the onset of convection during CO_2 sequestration. Transport in Porous Media 640, 441-452.

Ide, John M., (1936). "Comparison of statically and dynamically determined Young's modulus of rocks." Proceedings of the National Academy of Sciences of the United States of America 22.2.

Juanes, R.; Spiteri, E. J.; Orr, F. M., Jr.; et al., (2006). Impact of relative permeability hysteresis on geological CO_2 storage. Water Resour. Res. 42,Iss: 12 DOI: 10.1029/2005WR004806

Kano, Y., Funatsu, T., Nakao, S., Kusunose, K., Ishido, T., Lei, X.L., Tosha, T., (2013): Fault stability analysis related to CO_2 injection at Tomakomai, Hokkaido, Japan.Energy Procedia 37, 4946–4953.

Koh, J., Roshan, H., Rahman, S.S., (2011): A numerical study on the long term thermo-poro-elastic effects of cold water injection into naturally fractured geothermal reservoirs. Computers & Geotechnics 38, 669–682.

Loke, M.H., Barker, R.D., 1996. Practical techniques for 3D resistivity surveys and data inversion1. Geophysical Prospecting 44, 499-523.

Lonoy, A. (2006). Making sense of carbonate pore systems. AAPG Bull.90: 1381 – 1405

Lucia, F.J. (1983). Petrophysical parameters estimated from visual descriptions of carbonate rocks: a field classification of carbonate pore space .J. Petroleum Technol.pp. 629 – 637.

Lucia, F.J. (1999). *Carbonate Reservoir Characterization*, 226. New York: Springer.

Lucia, F.J. (1995). Rock-Fabric/Petrophysical Classification of Carbonate Pore Space for Reservoir Characterization. *AAPG Bull*. **79** (9): 1275-1300.

Lucia, F.J. (2007). Carbonate Reservoir Characterization Springer-Verlag, Berlin Heidelberg.

Luquot, L., and Gouze, Ph. (2009). Experimental determination of porosity and permeability changes induced by massive injection of CO_2 into carbonate reservoirs. *Chemical Geology*. doi:10.1016/j.chemgeo.2009.03.028 .

Luquot, L., Rodriguez, O. and Gouze, P. (2014a). Experimental characterization of porosity structure and transport properties changes in limestone undergoing different dissolution regimes. *Transport in Porous Media*, DOI: 10.1007/s11242-013-0257-4.

Luquot, L., Roetting, T. and Carrera J. (2014b). Characterization of flow parameters and evidence of pore clogging during limestone dissolution experiments. *Water Resources Research*. 50.

Martinez-Landa, L., Rötting, T., Carrera, J., Russian, A., Dentz, M., Cubillo, B., (2013). Use of hydraulic tests to identify the residual CO_2 saturation at a geological storage site. International Journal of Greenhouse Gas Control, Vol 19, pp 652-664, DOI: 10.1016/j.ijggc.2013.01.043.

Monier-Williams, M.E., Davis, R.K., Paillet, F.L., Turpening, R.M., Sol, S.J.Y., Schneider, G.W., (2009). Review of Borehole Based Geophysical Site Evaluation Tools and Techniques

Mousavi, M.A., M. Prodanović, D. Jacobi, (2013). New classification of carbonate rocks for process-based pore-scale modelling SPE Journal, 18, pp. 243–263

Neilson, J.E., N.H. Oxtoby, (2008). The relationship between petroleum, exotic cements and reservoir quality in carbonates – a review Marine and Petroleum Geology, 25 pp. 778–790

Nordbotten, J.M., Celia, M. and Bachu, S.. Injection and Storage of CO_2 in Deep Saline Aquifers: Analytical Solution for CO_2 Plume Evolution During Injection. Transp Porous Med (2005) 58:339–360. May 2004.

Pau, G.S.H., Bell, J.B., Pruess, K., Almgren, A.S., Lijewski, M.J., Zhang, K., 2010. High resolution simulation and characterization of density-driven flow in CO_2 storage in saline aquifers, Advances in Water Resources 33(4), 443-455.Peng D.Y., Robinson D.B., (1976). A new two-constant equation of state. Ind. Eng. Chem. Fundam. 15:59–64.

Pentland, C.H., El-Maghraby, R., Iglauer, S., Blunt, M.J., (2011). Measurements of the capillary trapping of super-critical carbon dioxide in Berea sandstone. Geophysical Research Letters 38.

Petrowiki website. Carbonate reservoir geology. http://petrowiki.org/Carbonate_reservoir_geology

Pruess, K. and Garcia, J. (2002): Multiphase flow dynamics during CO_2 disposal into saline aquifers. Environ. Geol. 42, 282–295

Redlich O., Kwong J.N.S., (1949). On the thermodynamics of solutions. Chem. Rev. 44:233-244.

Riaz, A, Hesse, MA, Tchelepi, HA and Orr, FM Jr, 2006. Onset of convection in a gravitationally unstable boundary layer in porous media. Transport in Porous Media 548, 87-111.

Rutqvist, J., Birkholzer, J.T., Cappa, F., Tsang, C.-F. (2007): Estimating maximum sustainable injection pressure during geological sequestration of CO_2 using coupled fluid flow and geo-mechanical fault-slip analysis. Energy Convers. Manage. 48, 1798–1807

Rutqvist, J., Dobson, P.F., Garcia, J., Hartline, C., Jeanne, P., Oldenburg, C.M., Vasco, D.W., Walters, M., (2013a): The Northwest Geysers EGS Demonstration Project, California: pre-stimulation modeling and interpretation of the stimulation. Mathematical Geosciences, http://dx.doi.org/10.1007/s11004-013-9493-9500 (in press).

Rutqvist, J., Cappa, F., Mazzoldi, A., Rinaldi, A., (2013b): Geomechanical modeling of fault responses and the potential for notable seismic events during underground CO_2 injection. Energy Procedia 37, 4774–4784.

Saaltink, M. W., Vilarrasa, V., De Gaspari, F., Silva, O., Carrera, J. & Roetting, T. S. (2013): A method for incorporating equilibrium chemical reactions into multiphase owmodels for CO_2 storage. Adv. Water Resour. 62, 431-441.

Schlumberger website. Carbonate reservoirs.
http://slb.com/services/technical_challenges/carbonates.aspx

Scholle, P.A. (1978): A color illustrated guide to carbonate rock constituents, textures, cements and porosities: AAPG Memoir 27.

Segall, P., Fitzgerald, S.D., (1998): A note on induced stress changes in hydrocarbon and geothermal reservoirs. Tectonophysics 289, 117–128.

Serra, O., (1984). 8. Neutron Logs, Fundamentals of Well-Log Interpretation — 1. The Acquisition of Logging Data. Elsevier, pp. 135-149.

Shalabi, Faisal I., Edward J. Cording, and Omar H. Al-Hattamleh, (2007). "Estimation of rock engineering properties using hardness tests." *Engineering Geology* 90.3.

Sheng, J., 2013. Enhanced Oil Recovery Field Case Studies. Gulf Professional Publishing, 772 pp.

Slichter, L.B., 1933. The interpretation of the resistivity prospecting method for horizontal structures. Journal of Applied Physics 4, 307-322.

Soave G., (1972). Equilibrium constants for modified Redlich-Kwong equation of state. Chemical Engineering Science 27:1196-1203.

Span R., Wagner W., (1996). A new equation of state for carbon dioxide covering the fluid region from the triple-point temperature to 1100K at pressures up to 800MPa. J. Phys. Chem. Ref. Data 25(6):1509-1596.

Szulczewski, Michael L.; MacMinn, Christopher W.; Herzog, Howard J.; et al. (2012). Lifetime of carbon capture and storage as a climate-change mitigation technology. Proceedings of the National Academy of Sciences of the United States of America, Vol: 109, Iss: 14 pp: 5185-5189 DOI:10.1073/pnas.1115347109

Van der Land, Cees, Rachel Wood, Kejian Wu, Marinus I.J. van Dijke, Zeyun Jiang, Patrick W.M. Corbett, Gary Couples, (2013). Modelling the permeability evolution of carbonate rocks, Marine and Petroleum Geology, Vol 48, December 2013, Pages 1-7

Vilarrasa, V., Bolster, D., Dentz, M., Olivella, S., Carrera, J., (2010). Effects of CO_2 compressibility on CO_2 storage in deep saline aquifers. Transp Porous Med 85, 619-639.

Vilarrasa, V., Carrera, J. and Olivella, S. (2012): Hydromechanical characterization of CO_2 injection sites. Int. J. Greenh. Gas. Control..

Vilarrasa, V., Silva, O., Carrera, J., Olivella, S., (2013a). Liquid CO_2 injection for geological storage in deep saline aquifers. International Journal of Greenhouse Gas Control 14, 84–96.

Vilarrasa, V., Carrera, J., Bolster, D., Dentz, M., (2013b). Semianalytical solution for CO_2 plume shape and pressure evolution during CO_2 injection in deep saline formations. Transp Porous Med 97, 43–65

Vilarrasa, V., Silva, O., Carrera, J., Olivella, S., Rutqvist, J., (2014). Long term impacts of cold CO_2 injection on the caprock integrity. International Journal of Greenhouse Gas Control 24, 1–13.

Wayne, M; Ahr (2011). Geology of Carbonate Reservoirs: The Identification, Description and Characterization of Hydrocarbon Reservoirs in Carbonate Rocks. Eds. John Wiley & Sons. 296 pp.

Wildgust, N., Tontiwachwuthikul, P. And Gilboy, C (Eds) (2013). The IEAGHG Weyburn-Midale Monitoring and Storage Project. International Journal of Greenhouse Gas Control, Volume 16 Supplement 1, 308pp.

Yamamoto, S., Miyoshi, S., Sato, S., Suzuki, K., (2013): Study on geo-mechanical stability of the aquifer-caprock system during CO_2 sequestration by coupled hydro-mechanical modelling. Energy Procedia 37, 3989–3996.

Yan and Thorin (2008): Process and Resource Optimization (PRO), Mälardalen University. Properties of CO_2/H_2O Mixtures with Impurities in Oxyfuel CCS Systems. Siemens Finspong Conference, Fingspång, April 9-10, 2008.

Zhang, Y.Q., Freifeld, B., Finsterle, S., Leahy, M., Ennis-King, J., Paterson, L., Dance, T., (2011). Single-well experimental design for studying residual trapping of supercritical carbon dioxide. Int. J. Greenh. Gas Control 5, 88-98.